Study of Sub-synchronous Resonance Oscillations in Wind Farms based on Variable Speed Wind Turbine Generators

by

Shi Tong

A thesis submitted in partial fulfillment of the requirements for the degree of

Master of Science

in
Energy Systems

Department of Electrical and Computer Engineering
University of Alberta

Abstract

In recent years, wind farms (WFs) based on variable speed wind turbine generators (VSWTGs) are occupying a significantly increasing market share due to the capability of controlling wind energy generation. The power control system in VSWTGs improves the wind energy conversion efficiency, while makes VSWTGs more vulnerable to break. Sub-synchronous resonance (SSR) oscillations have been observed in WFs based on VSWTGs, causing significant damage and performance degradation. Therefore, a comprehensive study of SSR oscillations in VSWTGs is presented in this thesis. Related research in terms of SSR analysis methods, the mechanisms and influence factors analysis and existing mitigation methods is carried out to proposed improved SSR mitigation schemes.

The behind root causes of SSR oscillations in WFs based on type 3 and type 4 WTGs are commonly believed to be the series capacitor compensation network and the weak grid condition, respectively. Rather than focusing the external grid condition, in the thesis, the inherent impedance property of WFs is addressed. A comprehensive study is carried on based on the impedance model of VSWTGs to find the internal mechanisms and impact factors of SSR oscillations in WFs based on VSWTGs.

Although different mitigation methods of SSR oscillations have been proposed as a result of the many studies, there is not a detailed study which analyzed and compared these methods. Consequently, the investigation of alternative approaches to mitigate and to optimize the existing solutions becomes challenging. To fulfil this gap, a comprehensive evaluation of the SSR mitigation strategies has been presented in this dissertation. And improved SSR damping schemes for WFs based on VSWTGs are proposed. The identified improved approaches are presented along with the time and frequency domain simulation results to validate their effectiveness.

Preface

This thesis is an original work by Tong Shi. The research project, of which this thesis is a part, received research ethics approval from the University of Alberta Research Ethics Board, Project Name "University of Alberta Future Energy Systems - Wind Farm Operation and Grid Integration (T14-P02)", which is leading by Professor Yunwei (Ryan), Li.

Chapter 3 and Sections 4.1 and 4.2 of the thesis is based on the paper submitted as **T. Shi**, Y.W. Li, D. Nayanasiri, "Sub-synchronous Resonance Oscillations in Wind Farms – An Overview Study of Mechanisms and Damping Methods", *IET Renewable Power Generation*. This paper is under review. I participated in the whole paper. I managed the paper, designed and did simulations, analyzed simulation results and contributed to the writing and editing of the manuscript.

Acknowledgements

The work presented in this thesis was carried out in the Electronic and Intelligent (ELITE) Grid Research Laboratory at University of Alberta.

I would like to express my deepest appreciation to my supervisor, Professor Yunwei (Ryan) Li for his invaluable guidance, generous support, and consistent kindness thorough the work. His unwavering enthusiasm for research helped make my time extremely productive. Without his patience, guidance, knowledge and assistance, this thesis would not have been possible.

I would like to thank Dr. D.R. Nayanasiri for his help in the paper and this thesis. I also would like to thank all my colleagues in ELITE Grid Research Laboratory, for many valuable discussions and joyful time that we shared together.

A very big thanks goes to my dear parents for understanding and supporting me all along. Thanks to my boyfriend, for always being by my side and inspiring me.

Table of Contents

List of Tables

List of Figures

Chapter 1
Introduction

Wind energy is one of the feasible alternative renewable sources to fulfil the energy demand while minimizing bad effects of traditional fossil energy sources. According to the global wind report 2018 published in April 2019 [1], the wind energy once again grew in strength in 2018. The wind energy industry now exists in more than 90 countries, 30 of which have more than 1,000 MW installed and 9 with more than 10,000 MW installed. Global wind energy council (GWEC) also forecasts that the increased wind installation would become 62.4 GW in 2022 and 62.6 GW in 2021. Today with the development of wind energy and power electric control technologies, an incredible amount of wind farms (WFs) have been constructed and integrated into the power grids.

Wind turbine generators (WTG), as an important part of WFs, extracts power from fluctuating wind and converts it into electrical energy. There are four main wind turbine generator (WTG) technologies, as shown in Fig. 1-1 [2]. Type 1 WTG is fixed-speed single cage induction generator (SCIG) based WTG, as shown in Fig. 1-1(a). In type 1 WTG no power converters are included. It has lower maintenance cost and reliable operation due to the simple power conversion configuration. But it is not able to control wind power generation due to lack to power converters. Besides that, it will suffer grid frequency stabilization issue when wind speed changes. Type 2 WTG, as shown in Fig. 1-1(b), is semi-variable-speed WTG and able to control a partial rated (10%) power flow due to the external resistor. Comparing with type 1 WTG, type 2 WTG has a higher energy conversion efficiency. But the external resistor will cause more system losses. Type 3 WTG, shown in Fig. 1-1(c), is variable-speed WTG which is able to control 25% of rated power generation due to the power converters between the rotor and external grid. It has a larger power control capability compared to type 2 WTGs. Type 4 WTG, shown in Fig. 1-1(d), is full-power generator which can be directly connected to the power system. The wind energy conversion efficiency of type 4 WTG is high due to the full variable speed range (0% - 100%). As reported in [2], in general, the most commonly installed technologies in today's systems are type 3 and type 4 WTGs. The biggest advantage of the WFs based on these variable speed WTGs (VSWTGs) is the facility to control the output and generation. However, the power electronics in control system

are vulnerable, and their damages would cause the breakdown of the whole WTG system. Therefore, the reliability and security of WFs-based on type 3 / 4 WTGs is critical.

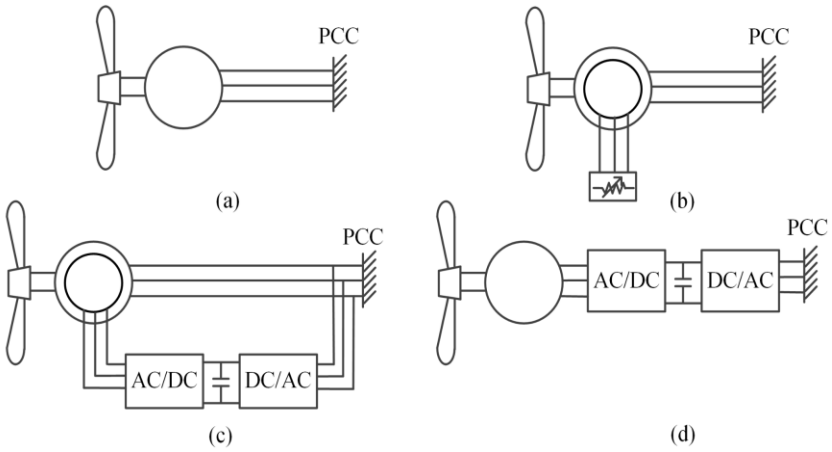

Fig. 1-1. The four wind turbine generator technologies,

(a) type 1 conventional induction generator, (b) type 2 variable rotor-resistance induction generation, (c) doubly-fed asynchronous generator, (d) type 4 full-converter generator [2].

The sub-synchronous resonance (SSR) oscillations are one of the identified causes behind the unavailability of the WFs because of the tripping. Moreover, SSR oscillations give rise to power quality issues in the power grid and further degrade system performance. Till now, the SSR oscillations have been observed in both type 3 (doubly-fed induction) and 4 (full power converter) generators causing much loss [3-11]. Therefore, a close analysis of the SSR oscillations, its root cause, effects on the system and mitigation methods would increase the reliability of the WF-based on VSWTGs, and consequently increase market penetration of the wind energy conversion systems.

In this dissertation, the investigation of the SSR problem in WFs based on VSTWGs are presented. Comprehensive work is carried out to analyzing the mechanism, impact factors, and to finding advanced alternatives to existing SSR mitigation methods.

This chapter starts with the introduction of basic SSR concept. Then the existing analysis methods of SSR oscillations are investigated and compared in detail. Next, a comprehensive review of the existing studies of SSR oscillations in type 3 and type 4 WTGs is then provided. Last, the objectives and organization of this dissertation is summarized at the end.

1.1 SSR definitions

The term SSR oscillations is defined in the IEEE committee report [12], i.e. "SSR is given power system condition where the electric network exchanges energy with turbine generator at one or more natural frequencies below the synchronous frequency". According to the definition, first and foremost, it should be considered that what kind of power system condition can generate SSR. As depicted in [12], any power system condition that allows exchange of energy at a given sub-synchronous frequency may experience SSR oscillations, e.g. the power system including series capacitor compensated transmission lines network. Next important factor to be considered is its origin. There are many ways in which the system and the generator can interact at sub-synchronous frequencies. They can be categorized as 1) the induction generator effect (IGE), 2) the torsional interaction (TI), and 3) the torque amplification (TA).

1.1.1 Induction generator effect (IGE)

The IGE is caused by self-excitation of the electrical system. Essentially it is brought by the fact that positive sequence sub-synchronous frequency (f_s) currents in the armature set up a rotating magnetic field which induces currents in the rotor of frequency (f_s - f_o, f_{so} denotes the fundamental frequency) [12]. The slip of the machine is

$$slip = \frac{f_s - f_o}{f_o} \tag{1-1}$$

According to (1-1), the slip is negative when the speed of magnetic field is slower than the rotor. Therefore, the resistance of the rotor to sub-synchronous current, seen from the armature terminals, is negative. Although the network presents a positive resistance to the sub-synchronous current going through it, if this negative resistance of the rotor to sub-synchronous current is greater in magnitude than the positive resistance of the network, there will be sustained sub-synchronous currents. Hence, due to this negative resistance, the system has a potential to be self-excited at sub-synchronous frequencies. Such self-excitation gives rise to excessive voltages and currents.

1.1.2 Torsional interaction (TI)

TI can be considered as the energy exchange between the series compensation network and mechanical parts of WTG, which is essentially an electro-mechanical phenomenon. TI occurs when the induced sub-synchronous torque in the generator is close to one of the torsional natural modes of the turbine-generator shaft. When the generator rotor oscillates at a torsional natural frequency (f_{mi}), voltage components at a frequency (f_{emi}) would be induced into the armature [12],

$$f_{emi} = f_o \pm f_{mi} \tag{1-2}$$

If f_{emi} is close to the SSR frequency, generator rotor oscillations will build up and this motion will induce armature voltage components at both sub-synchronous and super-synchronous. And the induced sub-synchronous frequency voltage is phased to sustain the sub-synchronous torque. And sub-synchronous torques will cause sustained mechanical oscillations on the rotor. However, the torsional natural frequency (f_{mi}) is quite low (1~5Hz), and corresponding f_{emi} is between 55Hz and 59Hz when the fundamental frequency is 60Hz. In WFs the SSR frequency usually does not appear in that high range. Therefore, for WFs, the TI may not be the concern.

1.1.3 Torque amplification (TA)

Both IGE and TI can be considered as the steady-state SSR, and TA is transient SSR which may result due to severe disturbance in the power system. After the severe disturbance happened in a power system, the sudden change of the rotor current will tend to oscillate at the natural frequencies of the network. In a transmission system without series capacitors, these transients are always dc, which will decay to zero with a time constant that depends on the ratio of inductance to resistance. For networks that contains series capacitors, the transient currents will contain one or more oscillatory frequencies that depend on the network capacitance as well as the inductance and resistance. If any of these sub-synchronous network frequencies coincide with one of the natural modes of a turbine-generator shaft, there can be peak torques that are quite large as these torques are directly proportional to the magnitude of the oscillating current. This is the root cause of TA.

From the above analysis we can see, the IGE is a purely electrical phenomenon only involving the rotor electrical dynamic. The TI comprises both the rotor electrical and mechanical dynamics and does more severe impacts than IGE. The TA exists as a result of the torque oscillation triggered by system disturbances. The existence of the SSR oscillation in the WFs based on fixed speed WTGs (FSWTGs - type 1 and type 2 WTGs) can be explained using the above categorization since

they are mainly due to the mechanical interactions [13-15], without the involvement of the power converters. However, this root cause identification cannot be employed to explain the behavior of the WFs based on VSWTGs.

By now, sub-synchronous control interaction (SSCI) [16] has been identified as one of the root causes behind the SSR oscillations in the WFs based on both type 3 and 4 WTGs. In the SSCI, there is no involvement of mechanical parts of the WTG system. The control system in type 3 and 4 WTGs are focused.

1.2 SSR analysis methods

In this section, the existing SSR analysis technologies are evaluated, which can be categorized into two categories: frequency-domain analysis methods (modal analysis, impedance model-based analysis and frequency-scanning method) and time-domain simulations. The modal analysis and the impedance model-based analysis are the most frequently used method in the literature. Therefore, a comprehensive analysis of both methods has been performed to identify the most suitable techniques to study SSR oscillations in WFs based on the VSWTGs.

1.2.1 Modal analysis

Modal analysis is a powerful tool to determine, improve and optimize dynamic characteristics of engineering structures. The modal analysis is based on the small-signal model of a linearized system. The small-signal model is utilized to analyze the dynamic properties of a system in the frequency domain. The modal analysis has been commonly used to study SSR oscillations in WFs. [12] and [50] provides a comprehensive explanation of its applications in power system to perform low-frequency oscillations and SSR oscillation analysis, respectively. When analyzing SSR oscillations, the modal analysis is able to provide a detailed description of the system to identify the frequencies and damping of oscillations in a specific SSR mode, to find influencing factors, and to design SSR damping controllers (SSRDCs) [17].

In modal analysis, three kinds of analysis can be utilized, i.e. Eigenvalue analysis, participation factors analysis, and residuals analysis, to obtain a detailed insight of the system. As explained in

[12], the eigenvalue analysis can provide a great insight into a system to identify the oscillation modes. As a result, SSR oscillation frequencies as well as the damping at corresponding frequency can be determined. The participation factors analysis measures the influence of each state of the system on different oscillation modes. This analysis helps identify the impact of the different system parameters on SSR oscillations. Finally, residuals analysis is employed to design the SSRDC, where residues reflect the influences of control parameters on the closed-loop control system [51].

In summary, the modal analysis provides a detailed description of the system having a deep insight about SSR oscillations. The quantitative information of a specific SSR mode provides information to determine the frequency and damping of oscillation, how multiple parameters influence SSR oscillations, and details to design SSRDCs. However, the modal analysis becomes complex and tedious when increasing the dimensions of the systems which should expect with the modern WFs. Moreover, the complexity of the system linearization process becomes high with increased system dimensions. Besides that, the calculation of the eigenvalues of a high dimension system needs significant computation power although there is a linearized system model. Despite performing modal analysis using advanced software tools like Matlab/SIMULINK and DIgSILENT/PowerFactory, it is difficult to obtain results with the required accuracy of a highly nonlinear system comprise many elements with nonlinear properties. Therefore, modal analysis has a limited capability to analyze modern WFs.

1.2.2 Impedance model-based analysis

Impedance model-based analysis has been successfully employed to study stability issues in dc-dc [52] and ac power systems [18] because it provides a clear picture of a system from an electrical perspective. Therefore, this method can be applied to analyze WFs based on type 3 and 4 WTGs because only the electrical part of the system involves giving rise SSR oscillations. This tool provides a detailed description of the system in an easily interpretable way to identify the root cause and influencing factors behind the SSR oscillations as explained in [5]. In addition to that, there is great flexibility in this method to extend an existing model of a system either adding more elements (such as STATCOM or HVDC systems) or changing control strategies. To be specific, a new model of a system can be obtained by independently changing the impedance model of the modified component. This is because modifications only involve a certain element of the entire

system. Besides that, the impedance models are accurate enough to describe the system properties under sub-synchronous frequencies. As a result, the overall system model has the required accuracy and might not suffer from the inaccuracies visible at the frequencies higher than half of switching frequency [55].

For both modal and impedance model-based analysis, there should be a linear time-invariant system since they are performed in the frequency domain using small-signal analysis. However, under certain circumstances, it may not feasible to obtain a linearized model as explained above. Therefore, in practical applications, the impedance model is obtained by simplifying the real system.

The impedance model is constructed either in the *dq* [19, 20, 23, 27-30, 32] or sequence synchronous [21, 56] reference frames. The following analysis can be performed after obtaining the impedance model: (1) resistance analysis (using the real part of the impedance model), (2) Bode plot, and (3) Nyquist's stability criteria. In the resistance analysis, the system resonance is identified using the sign of the equivalent resistance of the impedance model. A positive resistance stabilizes a system and a negative resistance makes the system unstable. The Bode plot reveals occurrence of SSR oscillations. To this end, the sub-synchronous frequency where two impedances (WF and the remaining system) having opposite properties can be detected. In this case, one system has a capacitive property and other shows an inductive property. The Nyquist's stability criteria is a frequently used method to identify SSR oscillations. To this end, the impedance model should be converted into either Thevenin or Norton equivalent forms as shown in Fig. 1 [24]. The voltage source shown in Fig. 1-2(a) should be stable when unloaded, and the condition stipulated in (1-3) should be satisfied. The condition in (1-4) should satisfy by the current source shown in Fig. 1-2(b) to have a stable operation. The Z_{WTG} and Y_{WTG} represent the equivalent impedance and admittance of the WTG, respectively. The Z_{Line} and Y_{Line} represent the equivalent impedance and admittance of the transmission line, respectively [24].

$$I(s) = \frac{V_s(s)}{Z_{WTG}(s) + Z_{LINE}(s)} = \frac{V_s(s)}{Z_{LINE}(s)} \frac{1}{1 + Z_{WTG}(s) / Z_{LINE}(s)} \tag{1-3}$$

$$V_s(s) = \frac{I(s)}{Y_{LINE}(s)} \frac{1}{1 + Y_{WTG}(s) / Y_{LINE}(s)} \tag{1-4}$$

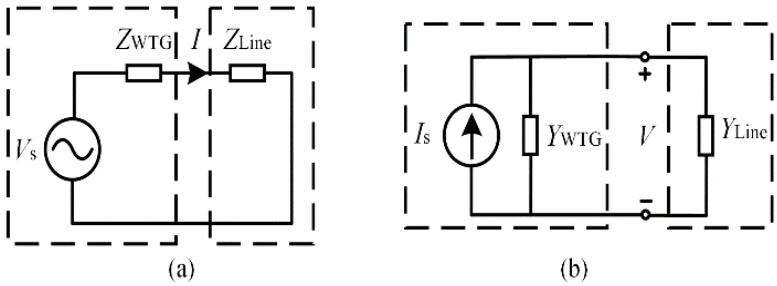

Fig. 1-2. Equivalent impedance model of WFs with external transmission lines (a) Thevenin equivalent, (b) Norton equivalent [22].

The system is stable when the number of counterclockwise encirclement around (-1 + j0) of the ratio term (Z_{WTG}(s)/Z_{LINE}(s)) in the denominator of (1-3), is equal to the number of zeros of Z_{WTG}(s)/Z_{LINE}(s) in the right-half complex plane minus the number of poles of Z_{WTG}(s)/Z_{LINE}(s) in the right-half complex plane. If all the poles of Z_{WTG}(s)/Z_{LINE}(s) are located in the left-half complex plane, then the system is stable if and only if there is no counter clockwise encirclement around (-1 + j0). In (1-4), the Nyquist's stability is determined by the ratio Y_{WTG}(s) / Y_{LINE}(s).

It is noteworthy that first, the above impedance model-based analysis can be directly applied to a SISO system having monotonous power sources to identify the root cause and impact factors of SSR. However, for a large system with different power sources, more advanced analysis methods like the generalized Nyquist criterion [68] or enhanced impedance analysis method [69] can be utilized to identify the resonance.

Second, the first two analysis methods, i.e. the real part of impedance model analysis and the bode plots analysis can provide a clear picture to system with feedback control systems, while the Nyquist's stability is utilized to check the stability of the system with open-loop control. As in this research, the impedance property of WFs are focused when studying SSR oscillations and the control systems are important parts in VSWTGs. Therefore, when find the mechanisms of SSR in WFs based on VSWTGs, it is assumed that the WFs with closed loop control can operate steadily at all frequency range and impedance property of WFs are analyzed under sub-synchronous frequencies.

1.2.3. Other analysis methods

There are two other analysis methods known as frequency scanning and time-domain simulation as summarized below.

1) Frequency scanning: This method provides a simple but effective way to analyze a non-linear system by linearizing the system at a given operating point. In the WF analysis, the impedance of the grid is examined at the point of common coupling (PCC) to detect the feasible frequency range, where SSR oscillations occur. A dip in the grid impedance curve plotted against frequency helps identify a relevant frequency range as explained in [3, 25]. In this method, WF is treated as a black box and use the harmonic injection method to obtain the grid impedance as a function of the frequency experimentally.

The frequency scanning analysis can be performed without a linearized small-signal model of the system when compared to the model-based analysis. However, this method does not help identify the influence of each component of the system to give rise to SSR oscillations. Also, this method cannot provide quantitative results, such as the specific SSR frequency or the SSR damping. Therefore, it is always used as a pre-detection method to identify the range of sub-synchronous frequencies and combined with other analysis methods (e.g. modal analysis), for further investigations [26].

2) Time-domain simulation: The model-based analysis should be performed in a wide operating rage since the WFs are non-linear systems. Therefore, in most papers, the IEEE first benchmark model (FBM) is adopted to perform nonlinear time-domain simulations to investigate SSR oscillations. A detailed description of the FBM is provided in [57], although it is criticized as a too simplified model to study SSR oscillations in real systems in [3] since there is no standard to design power converters in FBM.

A brief comparison between the SSR analysis methods is provided in Table 1-1. Comparing the advantages and disadvantages of each analyzing techniques, the impedance model-based method is selected for the remaining analysis of this paper.

Table 1-1. SSR analysis methods (√ indicates the method provides the information, x indicates the method is incapable).

	Modal analysis	Impedance model-based analysis	Frequency scanning	Time domain simulation
SSR frequency	√	√	√	√
SSR damping	√	√	×	×
Influence factors	√	√	×	√
Easily implement	×	√	√	√

1.3 Review of prior art for SSR in WFs based on type 3 and type 4 WTGs

There is a growing literature on the SSR oscillations in the WF based on type 3 and 4 WTGs to identify the root cause of the SSR oscillations, their effects, influencing factors and mitigation methods. They can be summarized in Table 1-2.

Table 1-2. A summary of the state-of-the-art SSR oscillation analysis and mitigation methods.

	WFs with type 3 WTGs	WFs with type 4 WTGs
Analysis methods	Modal analysis [17], impedance model-based analysis [4,18-24,27-32,56], frequency scanning [25,26], time-domain simulations [3].	
External causes	Series compensation [3-5] and HVDC transmission networks [11, 27]	Weak grid [6-10] and HVDC transmission networks [28-30, 64, 65]
Mitigation methods	1) Properly design the WTG system [31,32]. 2) Active use of power converters in WTGs [33-38]. 3) Add supplementary devices such as FACTS [39-47].	

The modal analysis [17], impedance model-based analysis [4,18-24], frequency scanning method [25,26], and time-domain methods [3] are the well-known techniques to analyze the SSR oscillation in the WF based on the VSWTGs. A qualitative and quantitative comparison between those techniques helps identify their strengths and weaknesses to have a deep insight into the problem to come up with effective alternatives to mitigate them.

Besides the SSCI, there are some alternative explanations behind the existence of the SSR oscillations in WFs based on VSWTGs as summarized in Table I. In [3-5], the existence of the SSR oscillations in WF based on type 3 WTGS has been explained as a result of the series compensation network. A weak grid connected to the WF based on type 4 WTGs has been identified as the reason in [6-10]. Moreover, an interaction between the HVDC transmission system and the WFs based on either type 3 or type 4 WTGs has been identified as another cause in [11,27-30,63,65]. However, neither analysis answers the question that although both type 3 and type 4 WTGs are VSWTGs, why they interact with external grids having different characteristics? Therefore, a thorough analysis focusing on the characteristics of WFs based on VSWTGs would help identify the real reason rather than considering the influence of the external grid.

Moreover, the most important topic in the engineer's perspective is the mitigation methods. SSR oscillations mitigation by the optimal parameter design [31, 32], using power converters in WTGs [33-38] and flexible alternating current transmission system (FACTS) controllers [39-47] have been proposed as summarized in Table 1-2. Each mitigation method has its own advantages and disadvantages and there is no publication compare their performance to identify the approach having the best damping performance. Therefore, a good comparison and evaluation of existing methods help researchers to find more efficient SSR oscillation damping methods and it is in the scope of this paper.

1.4 Objectives

In recent years, type 3 and type 4 WTGs acquire large market share and becoming most popular in WFs. And by now, SSR oscillations have been observed in WFs based on VSWTGs causing much damage. Therefore, it is important to investigate SSR mechanisms and mitigation methods in WFs, in order to guarantee the reliable and safe operation in WFs based on VSWTGs.

The main objectives of this thesis can be summarized as follows.

1) Investigation of SSR mechanisms

There are studies investigated the mechanisms of SSR oscillations in WFs based on type 3 and type 4 WTGs. As discussed in Section 1.2, it is commonly believed that the series capacitor compensation network and the weak grid condition are the root causes behind the SSR oscillations. But neither analysis answers the question, although both type 3 and type 4 WTGs are VSWTGs, why do they interact with external grids having different characteristics? Therefore, a thorough analysis focusing on the characteristics of WFs based on VSWTGs would help identify the root cause of SSR oscillations.

2) Improve Existing SSR mitigation schemes

Another important objective of this thesis is to improve the existing SSR damping methods used in WFs based on type 3 and type 4 WTGs. There are some popular SSR mitigation strategies, e.g. using power converters, utilizing flexible alternating current transmission system (FACTS) controllers, which have been discussed in Section 1.2. Each mitigation methods have their own advantages and disadvantages. Hence, a good comparison and evaluation of existing SSR mitigation schemes can help to find more advanced alternatives.

1.5 Dissertation Outline

This dissertation consists of six chapters which are organized as follows.

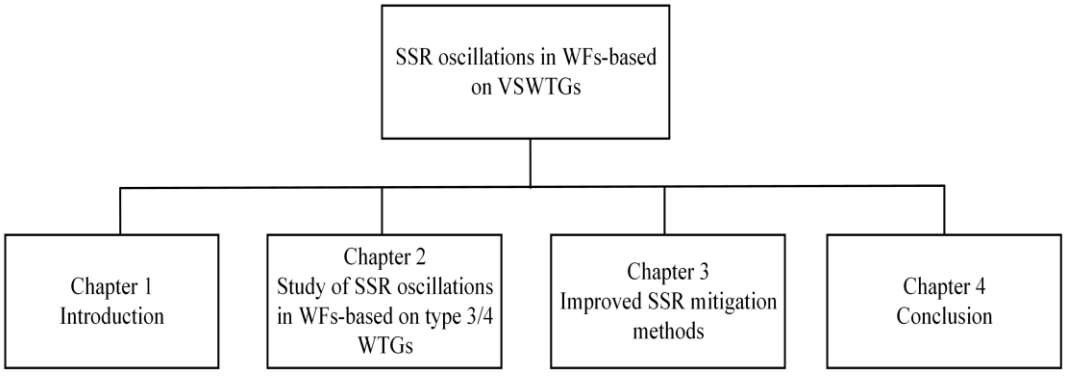

Fig. 1-3. Dissertation organization.

Chapter 1 presents the background and introduction of SSR concepts, analysis methods and existing studies of SSR in WFs-based on VSWTGs.

Chapter 2 investigates the SSR oscillations in WFs-based on type 3 WTGs and type 4 WTGs. In this chapter, several major aspects such as the mechanism, the influence factors and existing mitigation methods of SSR oscillations in WFs based on type 3 and 4 WTGs are investigated in detail. Besides, the SSR happened between the WFs based on VSWTGs and the high voltage DC (HVDC) transmission system are studied as well.

Chapter 3 focuses on the improvement of existing SSR mitigation schemes. It can be sub-categorized into two parts. In the first part, the improved SSR damping schemes are proposed by taking power converters and control strategies into consideration. To be specific, for WFs-based on type 3 WTGs, two types of improved SSR damping strategies are studied. They are parallel-connected virtual impedance control and STATCOM with SSRDC scheme. And for WFs-based on type 4 WTGs, all possible control strategies of GSC in type 4 WTG are studied in order to find the most suitable control methods to solve the SSR problem. In the second part, investigations about how to eliminate the impact of traditional PLL in SSR oscillations are addressed. First the problem of multiple SSR frequencies brought by the traditional PLL is studied. And then the modern PLL technologies are reviewed and compared. At last the suitable modern PLL technology is utilized to mitigate SSR oscillations. And relevant simulations are provided to prove the validity and effectiveness of the proposed SSR mitigation schemes.

Chapter 4 summarizes the main contribution and conclusion of the dissertation. Possible future research works are also suggested.

Chapter 2
Study of SSR in WFs based on VSWTGs

In this chapter, a comprehensive review of SSR in WFs based on VSWTGs and WFs with HVDC system are provided. Several major aspects including mechanism, the influence factors and existing mitigation methods of SSR in WFs based on VSWTGs are studied in detail. Relevant analysis in the frequency domain are provided by using impedance model-based analysis.

2.1 SSR in WFs based on Type 3 WTGs

SSR oscillations in WFs based on type 3 WTGs are investigated to identify the root cause, impact factors and mitigation methods of SSR oscillations. First, two real-world SSR oscillations in WFs based on type 3 WTGs to introduced, and selected as motivational examples to start the detailed analysis.

2.1.1 Two real-world examples

Two representative cases related to SSR oscillations in WFs based on type 3 WTGs have been reported by the Electric Reliability Council of Texas (ERCOT) system [3] and Hebei, China [4]. Most of the studies are based on these two study cases. A summary of these two cases are provided in Table 2-1. There is a significant difference in behavior due to the configurations of two WFs, such as different voltage/power ratings, control parameters, compensation levels of external series compensation networks and fundamental frequencies. A root cause identification behind SSR oscillations in WFs based on type 3 WTGs has been performed using the impedance model-based analysis along with the influencing factors in the following section.

Table 2-1. Two SSR oscillation case studies in WFs based on type 3 WTGs [3,4].

	WFs based on type 3 WTGs in ERCOT [3]	WFs based on type 3 WTGs in Hebei [4]
Power rating (MW)	/	88 ~ 360
Fund. frequency (Hz)	60	50

Compensation level (%)	75	6.67 (on average)
SSR frequency (Hz)	Around 20	6~8
SSR behaviors	The amplitude of oscillation overshot 150% of normal within in 200ms (growing fast).	The amplitude of oscillation reached to 125% of normal after 33s (growing slowly).

2.1.2 Mechanism of SSR in WFs based on type 3 WTGs

It is a well-known fact that SSR oscillation in WFs based on the type 3 WTGs is caused by the series compensation network. It can be intuitively explained using an equivalent impedance model of the WF, as shown in Fig. 2-1. Fig. 2-1(a) shows a power converter along with its control system. The equivalent impedance model of the WF is shown in Fig. 2-1(b). A detailed description of the impedance model of a WTG can be found in [19]-[23].

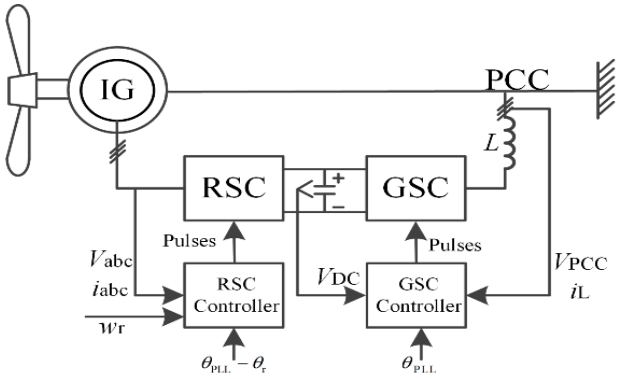

(a)

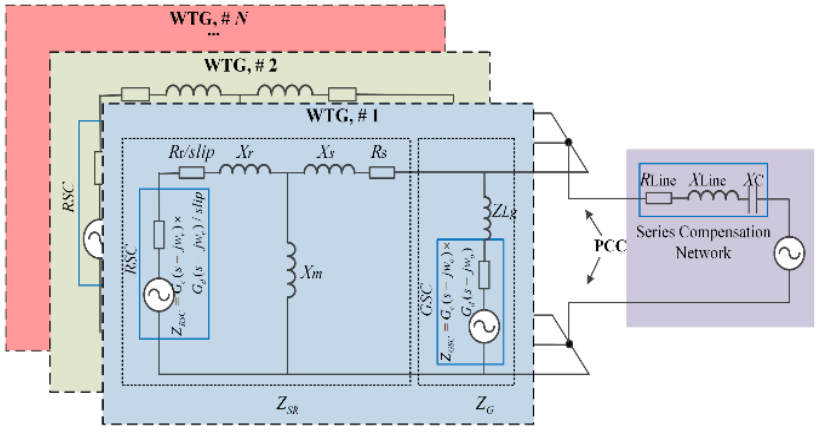

(b)

Fig. 2-1. WF based on the type 3 WTG (a) configuration of type 3 WTG, and (b) equivalent impedance model.

Type 3 WTG is modelled using two parallel-connected impedances Z_{SR} and Z_G; where Z_{SR} represents the impedance of rotor side converter (RSC) and induction generator (IG) and Z_G represents the impedance of the grid side converter (GSC) with a filter. The inner current loop and the control delay are considered when deriving the equivalent impedance of the RSC and GSC. However, the outer loop is not taken into consideration since the oscillations introduced by the outer torque loop is less than 1 Hz [33]. And the dynamics of interest are faster than that of the outer control loop. Therefore, the impedance model of the RSC and GSC are build neglecting the outer control. And the commonly used *dq*-based vector control is utilized as the starting point and then the model is transferred from *d*q reference framework to *abc* reference framework by replacing impedance $Z(s)$ with $Z(s\text{-}jw_o)$ where w_0 denotes angular speeds of the utility grid (377 rad/s). And the impedance model of RSC and GSC are given by (2-1) and (2-2), respectively; where, $G_c(s\text{-}jw_o)$ is the transfer function of the PI controller, and $G_d(s\text{-}jw_o)$ is the control delay, typically 1.5 times of sample period, and w_0 denotes angular speeds of the utility grid (377 rad/s).

$$Z_{GSC} = G_c(s - jw_o)G_d(s - jw_o) \tag{2-1}$$

$$Z_{RSC} = G_c(s - jw_o)G_d(s - jw_o) / slip \tag{2-2}$$

The equivalent impedances of the RSC with an IG (Z_{SR}) and GSC with an L filter (Z_G) are given by (2-3) and (2-4), respectively; where X_s and R_s denote the equivalent leakage inductance and resistance of the stator circuit and X_r and R_r denote the equivalent leakage inductance and resistance of the rotor circuit, X_m denotes the magnetizing inductance of the machine whose value is significantly larger than the X_s and X_r, and Z_{Lg} presents the impedance of the L filter. *slip* is the slip ratio defined in (2-5).

$$Z_{SR} = ((Z_{RSC} + R_r) / s + X_r) // X_m + X_s + R_s = R_{SR} + jX_{SR} \tag{2-3}$$

$$Z_G = Z_{GSC} + Z_{Lg} \tag{2-4}$$

$$slip = (w_0 - w_r) / w \tag{2-5}$$

The simplified equivalent impedance model of the WF is shown in Fig. 2-2(a). The equivalent impedance model including the WF consisting *n* number of type 3 WTGs as well as the external series capacitor compensation network. The equivalent RLC circuit of the WF and the series

capacitor compensation network shown in Fig. 2-2(b) can be used to explain the occurrence of the SSR oscillations between WF based on type 3 WTGs and the series compensation network.

$$Z_{DFIG} = (Z_{SR} // Z_G) / n = R_{DFIG} + jX_{DFIG} \tag{2-6}$$

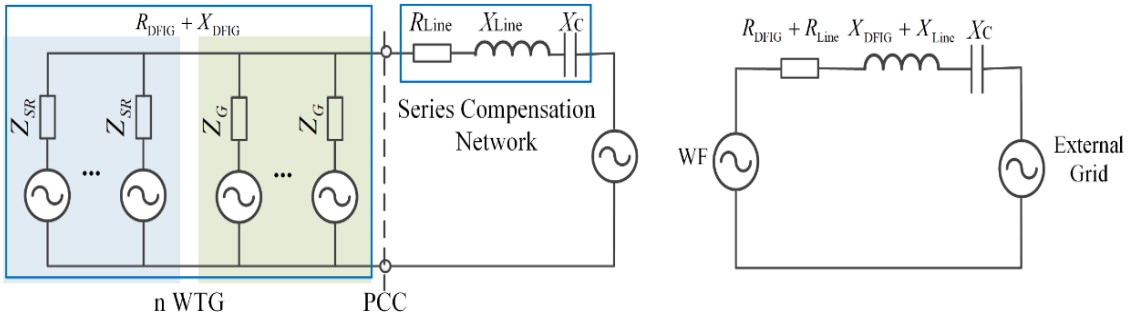

(a) (b)

Fig. 2-2. Equivalent impedance model of a WF with external series compensation network (a) simplified model, (b) equivalent RLC circuit.

The total equivalent resistance of the WF (R_{DFIG}) is negative when slip (*slip*) is negative at sub-synchronous frequencies. Therefore, the total resistance of the system becomes negative ($R_{DFIG} + R_{Line} < 0$) when the absolute value of R_{DFIG} exceeds the resistance of the external transmission line (R_{Line}). The oscillations generated by the inductive ($X_{DFIG} + X_{Line}$), capacitive (X_C) impedances of the system are amplified by that negative resistance giving rise system resonance. The corresponding sub-synchronous oscillation frequency can be obtained by (2-7) when $R_{DFIG} + R_{Line} << X$ and $R_{DFIG} + R_{Line} < 0$.

$$w_{sub} = w_o \sqrt{\frac{X_C}{X_{DFIG} + X_{Line}}} \tag{2-7}$$

The above analysis shows that the internal and the external root causes behind the SSR oscillation are the negative equivalent resistance of the RSC and IG combination, and the series compensation network, respectively.

2.1.3 Impedance model-based analysis

The above analysis can be supplemented using the bode and the resistance plots of a type 3 WTG obtained using (2-1)-(2-6). To this end, the transformation of three-phase variables into a rotating

dq reference frame is employed to model ac machines and converters. The impedance of the model in *dq* reference frame is given by (2-8).

$$\begin{bmatrix} \hat{V}_d(s) \\ \hat{V}_q(s) \end{bmatrix} = \begin{bmatrix} Z_{dd} & Z_{dq} \\ Z_{qd} & Z_{qq} \end{bmatrix} \begin{bmatrix} \hat{I}_d(s) \\ \hat{I}_q(s) \end{bmatrix} \tag{2-8}$$

The inner current loop of the RSC control system is only considered to obtain the model in (2-8). The outer control loop is ignored since the oscillations introduced by it less than 1 Hz [33] and the dynamics of interest are faster than that. Therefore, the outer control loop is considered as constant and has not been included in the impedance model [19]. In addition to that, symmetric property of the inner current loop in *d*- and *q*-axes help simplify the model in (2-8) using the relationships given by (2-9).

$$\begin{cases} Z_{dd} = Z_{qq} \\ Z_{dq} = Z_{qd} = 0 \end{cases} \tag{2-9}$$

The impedance model can be further simplified by representing it in the *abc* reference frame by replacing the *s* in (2-1)-(2-6) by (s-jw_0).

The obtained bode and the resistance plots of the impedance model of a WTG are shown in Figs. 2-3(a) and (b). The used simulation parameters are listed in Table. 2-2.

Table 2-2. The parameters of the SSR study model in time domain simulations.

	Parameters		Value (p.u.)
WF based on type 3 WTGs (P_{base}=2 MW, V_{base}=690 V, f_{base}=60Hz)	Power rating		1
	Voltage rating		1
	Rotor speed (w_r)		1.2
	Stator resistance (R_s)		0.023
	Stator inductance (L_s)		0.18
	Rotor resistance (R_r)		0.016
	Rotor inductance (L_r)		0.16
	Magnetizing inductance (L_m)		2.9
	RSC inner current controller	K_p	6
		K_i	8
	GSC inner current controller	K_p	0.83
		K_i	5
Series compensation network (P_{base}=100 MW, V_{base}=120 kV)	Series inductance (R_{Line})		0.5
	Series resistance (L_{Line})		0.02
	Compensated capacitance (L_C)		1/(0.1*0.5)
STATCOM/ESS (Q_{base}=3 MVar, V_{base}=25 kV)	L filter (L)		
	DC link voltage (V_{DC})		2400 V

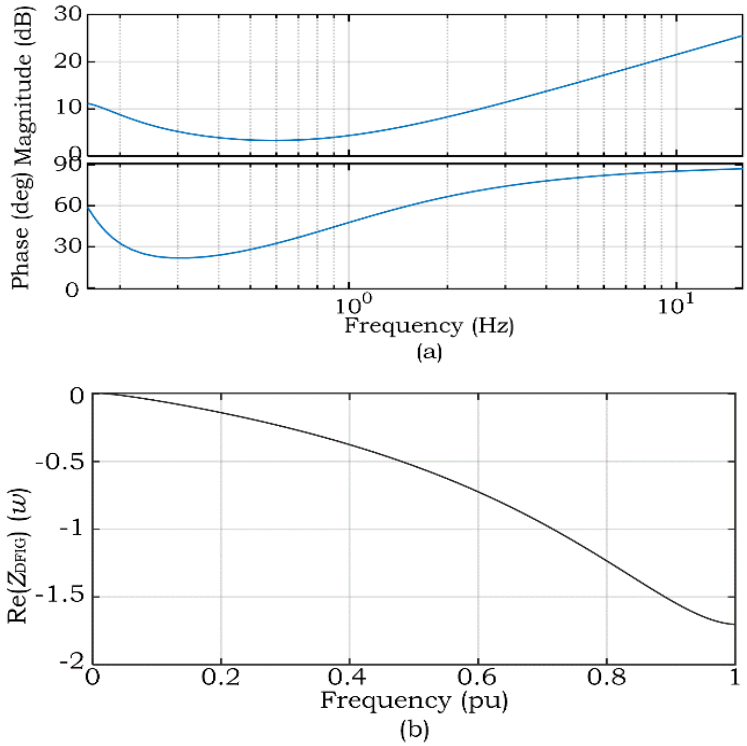

Fig. 2-3. Impedance analyses of type 3 WTG (a) Bode plot (b) real part (resistance) of the impedance model.

Fig. 2-3(a) shows that the phase angle of a type 3 WTG impedance model is always positive and behaves like an inductor. Fig. 2-3 (b) shows that the equivalent resistance is negative at sub-synchronous frequencies. As a result, the WF based on type 3 WTGs have a possibility to interact with the capacitive external systems. Moreover, SSR oscillations cannot be damped due to the negative equivalent resistance.

2.1.4 The effect of system parameters on SSR oscillations

The impact of system variables on the SSR oscillations can be investigated using the impedance model shown in Fig. 2-1(b). The transmission line resistance (R_{Line}) provides positive damping to SSR oscillations. However, large control parameters in both RSC and GSC controllers cause to have large negative damping in the WF based on type 3 WTGs (R_{DFIG}). As explained in [19], the magnitude of the equivalent impedance of a GSC with L filter (Z_{G}) is much larger than that of an RSC with an IG (Z_{SR}). The impact of the GSC branch behind the SSR oscillations can be neglected since Z_{G} is connected in parallel with Z_{SR}. Moreover, large wind speeds lead to a high absolute value of the slip ratio, according to (2-5), giving positive damping to SSR oscillations. According

to (2-6), the absolute value of equivalent resistance and inductance of the WF decrease when the number of parallel connected WTGs (n) goes high. The result is higher SSR oscillation frequency. Moreover, the relationship between the sub-synchronous oscillation frequency, the compensation level ($K = \frac{Z_C}{Z_L}$) and fundamental frequency (f_o) can be deduced using (2-7). These facts are summarized in Table 2-3.

Table 2-3. The effects of systems parameters on the SSR oscillations in WF based on type 3 WTG [4,5], [17], [23].

Cause		Effect
Series compensation network	Compensation level	Large compensation level leads to high SSR frequency [4,5,23].
	Line resistance	Large line resistance provides positive damping to SSR oscillations [5].
Wind speed		Fast wind speed provides positive damping to SSR oscillations [4,5,17,23].
WF parameters	RSC controller	Large control parameters provide negative damping to SSR oscillations [5,17].
	Number of WTGs	Large number of WTG moves the SSR frequency higher [4,5].

2.1.5 Existing mitigation methods for WFs based on type 3 WTGs

There are two most frequently used SSR mitigation methods; 1) employing flexible alternating current transmission system (FACTS) controllers, and 2) actively using power converters of WTG. The essential of these two methods is to introduce additional damping into the system, which can be obtained either utilizing SSR damping controller (SSRDC) [33-36,40-45] or virtual impedance [37]. The typical configuration of an SSRDC is shown in Fig. 2-4 and it is essentially a power system stabilizer (PSS). The SSRDC samples the voltage at PCC. The generated auxiliary damping signal by SSRDC is fed into the existing control loops of FACTS controllers or to the GSCs of WTGs. The virtual impedance method is implemented by introducing additional feedback loops (either coupling back line-voltage or current) into existing controllers [58]. It is usually embedded into the GSC in WTGs.

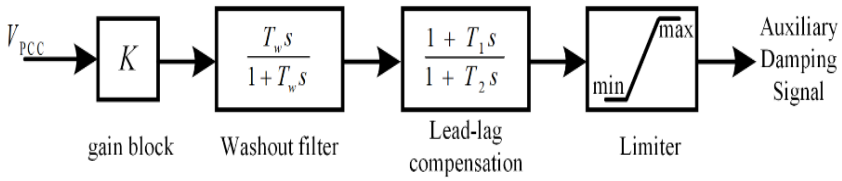

Fig. 2-4. Structure of the SSRDC.

1) Utilizing FACTS Controllers

In FACTS controllers, a thyristor-controlled series capacitor (TCSC) provides damping to SSR oscillations without using an auxiliary SSRDC. The TCSC is capable to boost power transfer capability into the transmission line as the conventional compensation network, while TCSC can provide positive resistance to damp SSR oscillations at the sub-synchronous frequencies [39]. SSR damping performance can be further improved through integrating additional SSRDCs in the control system of TCSC as proposed in [40]. A gate-controlled series capacitors (GCSC) with an additional SSRDC has similar SSR damping performance like a TCSC with an SSRDC [41,42]. Although the series-connected FACTS controllers have a significant SSR oscillations damping performance, their implementation may not be as simple as shunt connected FACTS controllers such as static var compensator (SVC) and static synchronous compensator (STATCOM).

STATCOM, the most widely used FACTS controller, has been successfully employed to mitigate SSR oscillations. STATCOMs are used in WFs to compensate dynamic reactive power and support voltage in the existing systems. Therefore, additional SSR damping function can be introduced into the control system without additional construction cost. Such SSR mitigation scheme has been realized by adding auxiliary SSRDC signals to either *d*- or *q*-axis of the STATCOM control loop in [43-45]. In most papers, the additional damping signal is added into the *q*-axis of the control loop, as shown in Fig. 2-5.

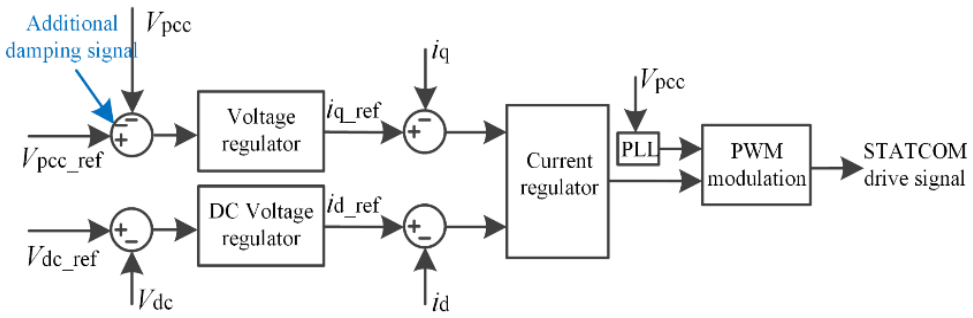

Fig. 2-5. *q*-axis of STATCOM control loop with additional SSR damping signal.

SSR damping performance of the classical STATCOM with SSRDC has been further improved using additional damping introduced into the control loop via a virtual impedance in [46]. In [47], a fuzzy logic (FLC) and an adaptive neuro-fuzzy inference system (ANFIS) controllers have been employed to generate an auxiliary damping signal.

2) Utilizing Power Converter of WTGs

Damping can also be integrated into the system using the power converters of WTGs. As discussed previously, parameters of the RSC controller should be as small as possible since it has a negative effect on system resonance. Therefore, in most cases, the GSC of WTGs is utilized to integrate additional SSR damping signals. The auxiliary SSR damping signal can be generated either using an SSRDC [33]-[36] or using the virtual impedance control method [38].

Fig. 2-6 shows the configuration of GSC with auxiliary SSR damping signal introduced by SSRDC. The additional SSR damping generated by SSRDCs is introduced into the reactive power control loop of the GSC in [34,35] and into both the reactive power and DC-link voltage control loop [33]. In [36, 59], the most suitable point to introduce the SSR damping term has been investigated. The *d*-axis of the GSC control loop is selected as the most suitable point to introduce the additional SSR damping signal.

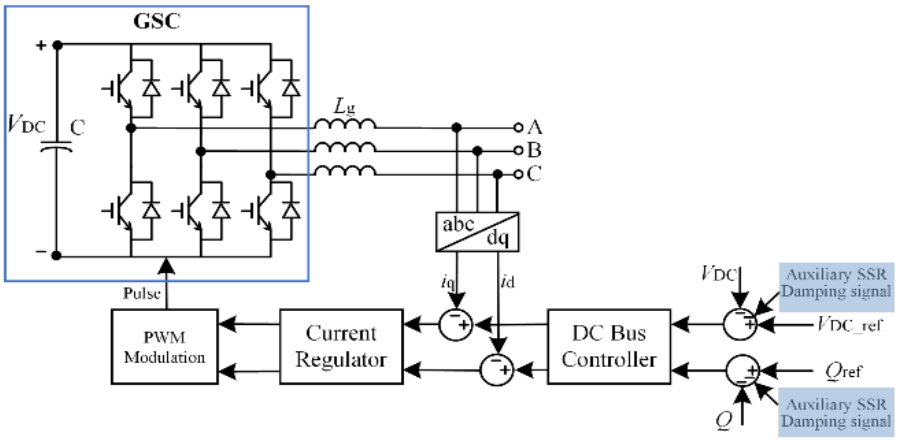

Fig. 2-6. Configuration of GSC with auxiliary SSR damping signal.

One of the necessary conditions to exist SSR oscillation is negative equivalent resistance in the overall system. Therefore, SSR oscillations can be avoided by controlling the overall system impedance to be positive using virtual impedance control. The virtual impedance method introduces additional impedance into the system, to provide additional damping. The realization of virtual impedance control has been demonstrated in [37], as shown in Fig. 2-7.

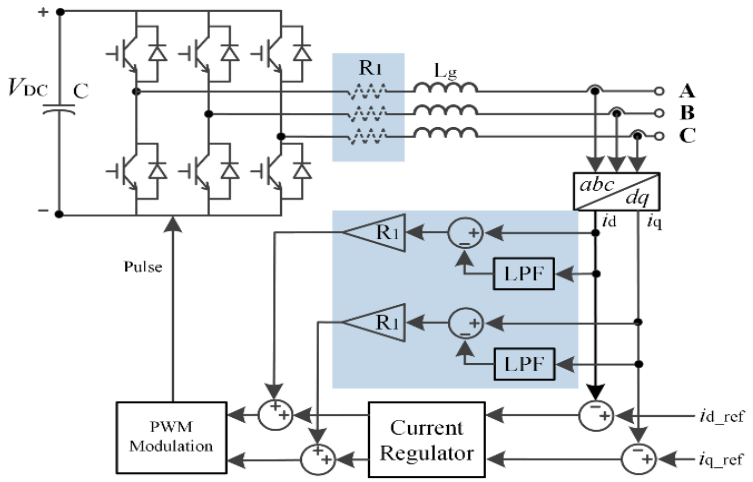

Fig. 2-7. Configuration of GSC with additional virtual impedance control [35].

In the next chapter, the above two SSR oscillation mitigation methods; 1) using STATCOM and 2) using virtual impedance control are studied and compared in detail. Their existing shortcomings and pointed out and possible approaches to improve the performance are investigated and validated using both frequency and time-domain simulations.

2.2 SSR in WFs based on Type 4 WTGs

A well-known case study had been reported in Xinjiang, China, in July 2015. The SSR oscillations in the reported trip three 600 MW WFs [6-9]. There was no series compensation network connected to the WF and the observed SSR oscillation components were at 19.4, 29.6, 39.8 Hz [10] frequency bands. According to [6-9], the root cause behind SSR oscillations is a weak AC grid. Next, based on this study case, the mechanism of SSR oscillations in WFs based on type 4 WTGs will be analyzed. And the impact factors and mitigation schemes are carefully analyzed to find a potential improved mitigation method.

2.2.1 Mechanism of SSR in WFs based on type 4 WTGs

The impedance model-based analysis is utilized to identify the mechanism behind the SSR oscillations in WFs based on type 4 WTGs. The typical configuration of a type 4 WTG with back-to-back power converters is shown in Fig. 2-8(a). Type 4 WTGs, as a VSWTG, are operated at an optimal rotation speed as a function of the wind speed. The machine side converter (MSC) typically extracts the maximum possible power using a maximum power point tracking (MPPT) algorithm. The GSC maintains a constant DC-link voltage and supplies the active nominal power to the grid. There are no direct interactions between the generator and the transmission network due to the DC-link capacitor of the power converter. Fig. 2-8 shows the equivalent model of such a system, which is obtained only considering the GSC.

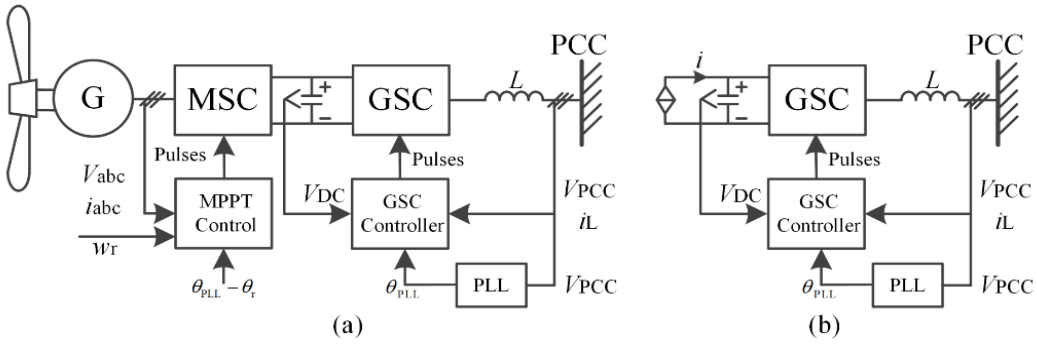

Fig. 2-8. A type 4 WTG (a) configuration of the control system (b) the simplified system using the equivalent model of the generator.

A complete description of the impedance model of the type 4 WTG can be found in [30,51,52]. The impedance model should be constructed using the *dq* reference frame due to the asymmetrical structure in the *d*- and *q*-axes of the GSC of the type 4 WTG. The simplified equivalent impedance model of a type 4 WTG is given by (2-9); where R_{PMSG} is the negative equivalent resistance of the WTG, X_{PMSG} is the large but negative (capacitive) equivalent impedance [5], and n is the number of WTGs.

$$Z_{PMSG} = (R_{PMSG} + jX_{PMSG}) / n \tag{2-9}$$

Therefore, SSR oscillations would emerge in a system including WFs with type 4 WTGs and weak AC grid having inductive impedance characteristics [5-7, 29]. Comparing WFs based on type 3 WTGs with WFs based on type 4 WTGs, we can find that the root cause behind the SSR oscillations can be identified as the negative equivalent resistance of the WFs based on either type 3 or type 4 WTGs. The negative resistance is due to the slip ratio (*slip*) in the IGs of type 3 WTGs, and caused by the impedance characteristics of VSCs in type 4 WTGs. The equivalent impedance of two types of WFs has different properties, where it is inductive in WF based on the type 3 WTG, and it is capacitive in WF based on the type 4 WTG. Therefore, external factor gives rise to the SSR oscillations in type 4 is a weak grid although it is due to the series compensation network in the type 3 WTG system.

2.2.2 Impedance model-based analysis

As explained above, the equivalent impedance model of a type 4 WTG can be obtained considering only the model of the GSC. Figs. 2-9(a), (b), (c), (d) and (e) show the configurations of the current controller, DC voltage controller, reactive power controller and ac voltage controller in the control system of a type 4 WTG, respectively. This impedance model is built based on the impedance model of VSC in [32,53,54].

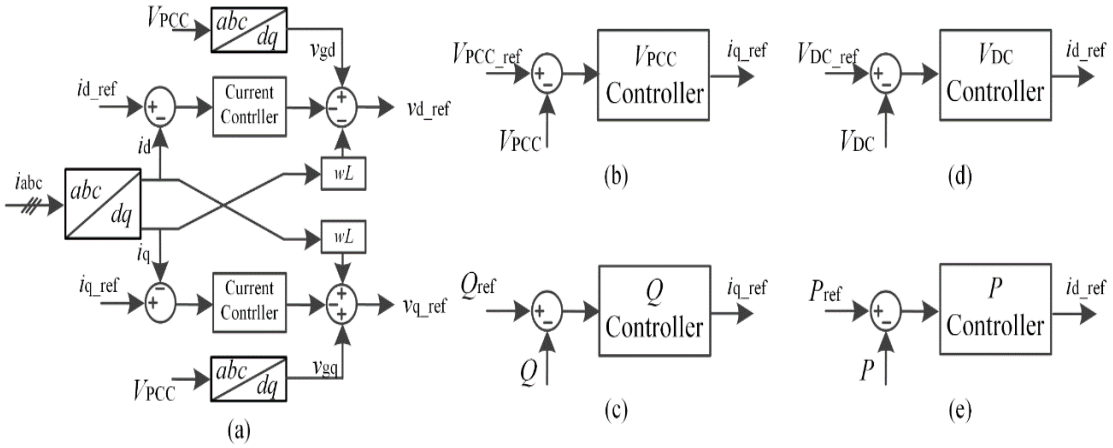

Fig. 2-9. Configuration of controllers in GSC, (a) Current controller, (b) V_{PCC} controller, (c) Q controller, (d) V_{DC} controller, and (e) P controller.

The increments of the reference current on the d-axis when the outer control loop adopts V_{DC} control.

$$\Delta i_d^{ref} = T_1' \Delta v_{gd} + T_2' \Delta v_{gq}$$
$$T_1' = \frac{-((V_{PCC\_ref})^2 y_i(s) + P_{ref}) C_{DC}}{s V_{PCC\_ref} C_{DC} V_{DC\_ref} + (V_{PCC\_ref})^2 V_{PCC\_ref} C_{DC}} \text{ and } T_2' = \frac{-Q_{ref} C_{DC}}{s V_{PCC\_ref} C_{DC} V_{DC\_ref} + (V_{PCC\_ref})^2 V_{PCC} C_{DC}} \quad (2\text{-}10)$$

where C_{DC} denotes the PI controllers of the outer DC voltage loop.

The increments of the reference current on the d-axis when the outer control loop adopts P control.

$$\Delta i_d^{ref} = T_1' \Delta v_{gd} + T_2' \Delta v_{gq}$$
$$T_1 = -\frac{P_{ref}}{(V_{PCC}^0)^2} \text{ and } T_2 = 0 \quad (2\text{-}11)$$

The increments of the reference current on the q-axis when the outer control loop adopts V_{PCC} control.

$$\Delta i_q^{ref} = F_1 \Delta v_{gd} + F_2 \Delta v_{gq}$$
$$F_1 = -C_{PCC} \text{ and } F_2 = 0 \quad (2\text{-}12)$$

where C_{PCC} denotes the PI controllers of the outer V_{PCC} loop.

The increments of the reference current on the q-axis when the outer control loop adopts Q control.

$$\Delta i_q^{ref} = F_1'\Delta v_{gd} + F_2'\Delta v_{gq}$$
$$F_1' = C_Q\left\{\frac{Q_{ref}/V_{PCC\_ref}}{1-V_{PCC\_ref}C_Q f_{cc}}\right\} \text{ and } F_2' = C_Q\left\{\frac{P_{ref}/V_{PCC\_ref} + Z_{cc}^{-1}V_{PCC\_ref} - P_{ref}/V_{PCC\_ref}G_{PLL}}{1-V_{PCC\_ref}C_Q f_{cc}}\right\} \quad (2\text{-}13)$$

where C_Q denotes the PI controllers of the outer reactive voltage loop. f_{cc} denotes the transfer function of the inner current loop.

The traditional GSC of type 4 WTG controls PCC voltage (V_{PCC}) using q-axis and DC-link voltage (V_{DC}) using d-axis. Hence, the impedance model of the GSC can be built using Figs. 2-9(b) and (d). In this section, only the resistance property will be discussed, and the detailed discussion on the impedance property based on the bode plot will be presented in detail in Chapter 3.

Fig. 2-10 shows the real part of the impedance model. The real part of impedance Z_{dd}, Z_{dq}, Z_{qd} and Z_{qq} is negative at sub-synchronous frequencies.

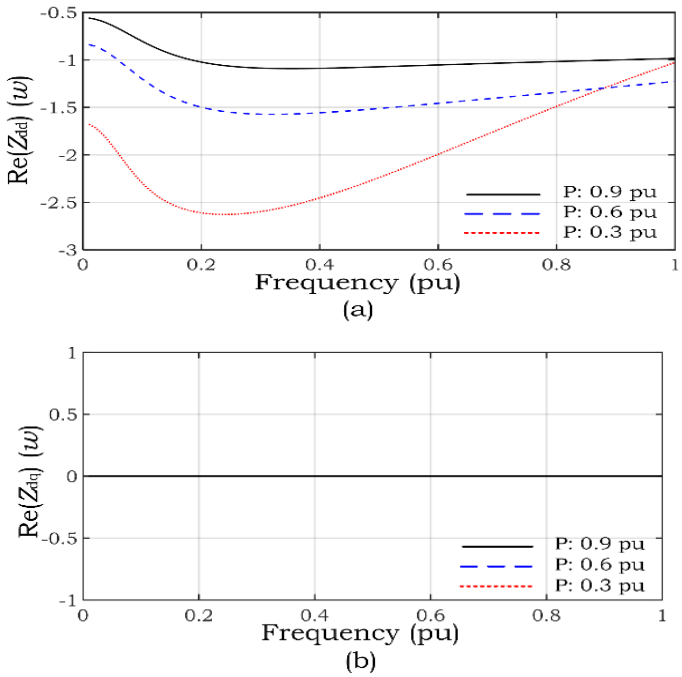

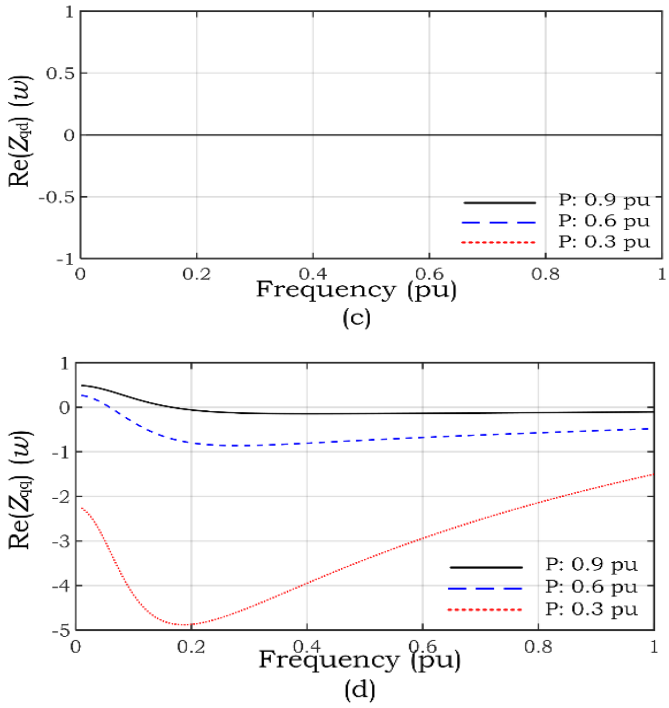

Fig. 2-10. Plots of real part of impedance model of a type 4 WTG with different power rating (a) Z_{dd} (b) Z_{dq} (c) Z_{qd} (d) Z_{qq}.

It can be found from Fig. 2-10 that the equivalent impedance model of the type 4 WTG has a negative resistance and capacitive reactance. As the power rating increases, the negative resistance increases. Therefore, the WFs based on type 4 WTGs may interact with the weak grid under sub-synchronous frequencies to give rise oscillations which cannot be damped due to the negative resistance.

2.2.3 The effect of system parameters on SSR oscillations

The observations of the impedance model-based analysis are summarized in Table 2-4 to identify the influencing factors.

Table 2-4. SSR Influence Factors in WFs based on Type 4 WTGs [8, 10, 60, 61].

System variables	Influence
Grid impedance	Large grid impedance makes the SSR frequency lower and SSR oscillations more serious [8].
Wind speed	Fast wind speed provides positive damping to SSR oscillations [8, 60].
Number of WTGs	Large number makes the SSR frequency lower and provides negative damping to SSR oscillations [8].

WTG control parameters:	
DC voltage measurement delay	Large delay time makes the SSR oscillations more serious [60].
Three PI controllers	I term in V_{DC} and in q-axis current controllers provide negative damping [8]. P term in d-/q-axis of current controllers provide negative damping [8]. P term in V_{DC} and I term in d-axis current controllers provide non-monotonic damping [8].
Reactive power injection	Reactive power provides positive damping [10].
PLL block	SSR oscillations at multiple frequencies, makes the system more unstable [8, 61].

According to the summary provided Table 2-4, the wind speed provides positive damping to SSR oscillations in WFs based on type 4 WTGs. Fast wind speed makes the system less vulnerable to SSR oscillations. The number of WTGs has a different impact on the WF based on the type 4 WTGs. The SSR oscillations frequency is high in WFs based on type 3 WTGs where there is a larger number of WTGs. However, there is an opposite trend in the systems based on type 4 WTGs. Besides that, the number of WTGs has a nonlinear impact on the damping of SSR oscillations in WFs based on type 3 WTGs [5]. The relationship between the number of WTGs and damping of SSR oscillations are negatively correlated in WFs based on type 4 WTGs [8]. It is noteworthy that when analyzing the impact of the number of PMSGs, the short circuit ratio (SCR) should also be taken into consideration as explained in [8].

In Section 3.1, the impact of the PLL block of the controller has not been taken into consideration as the influence of GSC of WTG control system behind the SSR oscillations can be neglected. However, in type 4 WTGs the impact of PLL block in the GSC should not be neglected. For example, the SSR oscillations at multiple resonance frequencies due to the PLL block has been discussed in [10, 61]. When a signal at the sub-synchronous frequency w_s is fed into the PLL block, the output of PLL block contains harmonics at (w_0 - w_s) and 2(w_0 - w_s) giving rise harmonics at frequencies w_s, 2w_0 - w_s, w_0 – 2w_s, 3w_0 - 2w_s. All these harmonics negatively affect PLL performance and generate SSR oscillations at frequencies w_s, 2w_0 - w_s, w_0 – 2w_s, 3w_0 -2w_s, 2w_0 - 3w_s, 4w_0 -3w_s, 3w_0 -4w_s, 5w_0 -4w_s,.. As explained in [6], the outer control loops of GSC impact SSR oscillations, and in Chapter 3 more comprehensive discussion about the impact of outer control loops of GSC will be presented.

2.2.4 Existing mitigation methods for WFs based on type 4 WTGs

One alternative to damp SSR oscillations is optimizing the control parameters of the GSC. Such optimization can be performed to reshape the equivalent impedance characteristics of type 4 WTGs to avoid the SSR oscillations [31]. In [32], the delay time of dc voltage measurement has been identified as a reason to increase the SSR oscillations. Therefore, authors have suggested reducing the measurement delay time using proved sampling, filtering and processing methods.

Another alternative would be active use of GSCs to provide additional SSR damping. This idea has been proposed in [7,32], which is similar to the case of WFs based on type 3 WTGs. In [61], authors have proposed an active damping impedance control method to reshape the impedance property of GSC, which is very similar to the virtual impedance method discussed in Chapter 2. The virtual impedance method is not capable to mitigate the SSR in WFs based on type 3 WTGs since the large IG impedance dominates the total impedance of the WF system. Therefore, adding positive damping by increasing the equivalent resistance of the WF system through the controller may not solve the problem. However, IG does not appear in the system impedance model of type 4 WTG. As a result, the virtual impedance model can achieve satisfactory damping performance in WFs based on type 4 WTG as demonstrated in [62].

In addition to that, supplementary STATCOM devices can be used to damp SSR oscillations. Author of [7] has suggested using a STATCOM to operate in reactive power control mode to damp SSR oscillations.

2.3 SSR between WFs and HVDC systems

In this section, an in-depth analysis of SSR oscillations in the systems consists of WFs based on VSWTGs and HVDC is provided. As the available literature in this area is mainly based on the VSC-HVDC systems. Therefore, the root cause of SSR oscillations in the interconnected system containing WFs and HVDC is analyzed by employing the impedance model-based. In addition to that, the existing mitigation methods will also be analyzed to identify their limitations to find improved alternatives.

A real-world example of the SSR oscillations observed in a modular multi-level converter and high voltage dc (MMC-HVDC) system has been reported in [11]. The WTGs of that systems are based on type 3 and type 4. SSR oscillations at 21 Hz had been observed when each type of WF was separately connected to the sending end converter (SEC) of MMC-HVDC transmission system.

2.3.1 Mechanism of SSR in WFs with HVDC connection

By now, a few case studies can be found in the literature [11], [27-30, 64,65] related to the SSR oscillation in these systems. In [11] and [27], the appearance of the SSR oscillations, and its distribution and propagation between SEC and REC side of the MMC-HVDC in WF based on type 3 WTG has been discussed with a detailed analysis. The SSR oscillations in a similar HVDC system but connected to the type 4 WTGs have been studied in [28-30, 64, 65]. In these publications, WFs are connected to the SEC of the HVDC system, and the appearance of SSR oscillations have been explained as a result of the interaction between GSC of WTGs and SEC of HVDC system.

Impedance model of a WF based on type 3 WTG can be modelled using a negative resistance with an inductive reactance in series, and it is negative resistance with a capacitive reactance connected in series when considering a WF based on type 4 WTGs. Hence, there is a potential to interact WFs based on both type 3 and type 4 WTGs [11, 27-30, 64, 65] with HVDC system to give rise SSR oscillations since the equivalent impedance of HVDC system could be either inductive or capacitive. Therefore, the impedance properties of HVDC systems have been investigated to further validate this assumption. To this end, existing HVDC system control strategies have been studied. Fig. 2-11 shows the configuration of an HVDC control system. As discussed in [66], one terminal maintains the DC-link voltage while another terminal regulates the power flow in conventional systems. Typically, the SEC controls the V_{PCC} and P [11, 27-30, 64, 65].

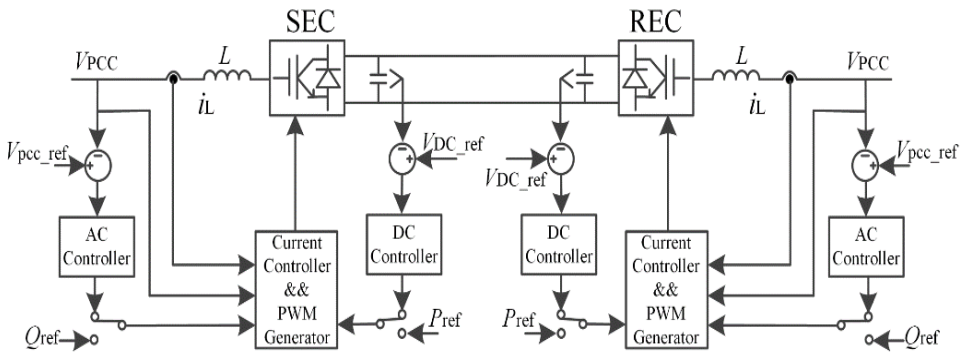

Fig. 2-11. Configuration of a HVDC transmission system.

2.3.2 Impedance model-based analysis of SSR oscillations in WFs with HVDC connection

The impedance property of HVDC-SEC is studied based on two models. First, the impedance model of the SEC is obtained assuming the traditional control strategy of SEC-HVDC using the models provided in Figs. 2-9(b) and (e). Since the HVDC-connected WFs can be operated as islanded grid, the SEC should control the AC grid voltage and frequency. So, the impedance model of SEC is constructed when it controls the V_{PCC}.

The Bode plots of the system when the HVDC-SEC controls P and V_{PCC} are shown in Fig. 2-12 and the observations can be summarized as follows.

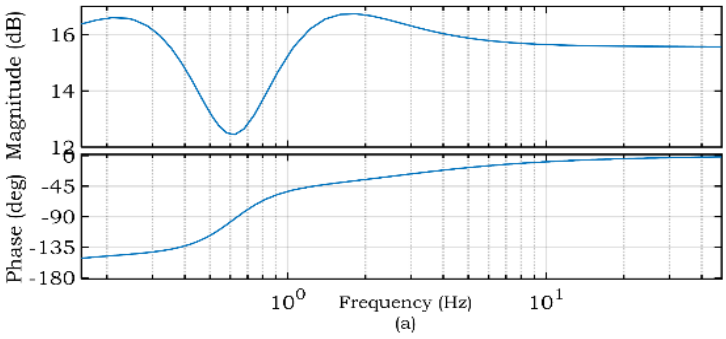

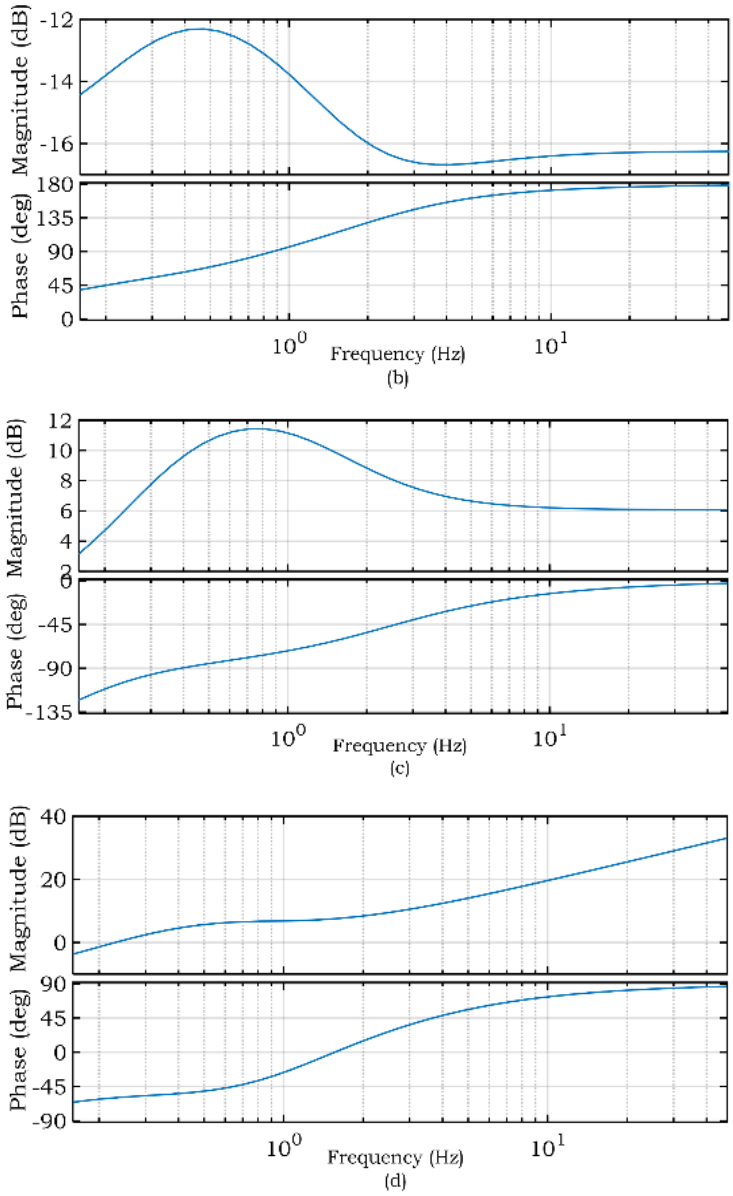

Fig. 2-12. Bode plots of the equivalent impedance of the HVDC-SEC (a) Z_{dd} (b) Z_{dq} (c) Z_{qd} (d) Z_{qq}, when the HVDC-SEC controls P and V_{PCC}.

Fig. 2-12 shows that;1) Z_{dd} and Z_{qd} is capacitive at all sub-synchronous frequencies, 2) Z_{dq} is inductive at all sub-synchronous frequencies 3) Z_{qq} is capacitive at low frequencies (<1 Hz) and becomes inductive when the frequency is higher than 1 Hz. Therefore, HVDC-SEC with P and V_{PCC} control strategy has an inductive or capacitive property which might interact with WF based on type 3 and 4 WTGs.

The Bode plots of the system when the HVDC-SEC controls V_{PCC} are shown in Fig. 2-13 and the observations can be summarized as follows.

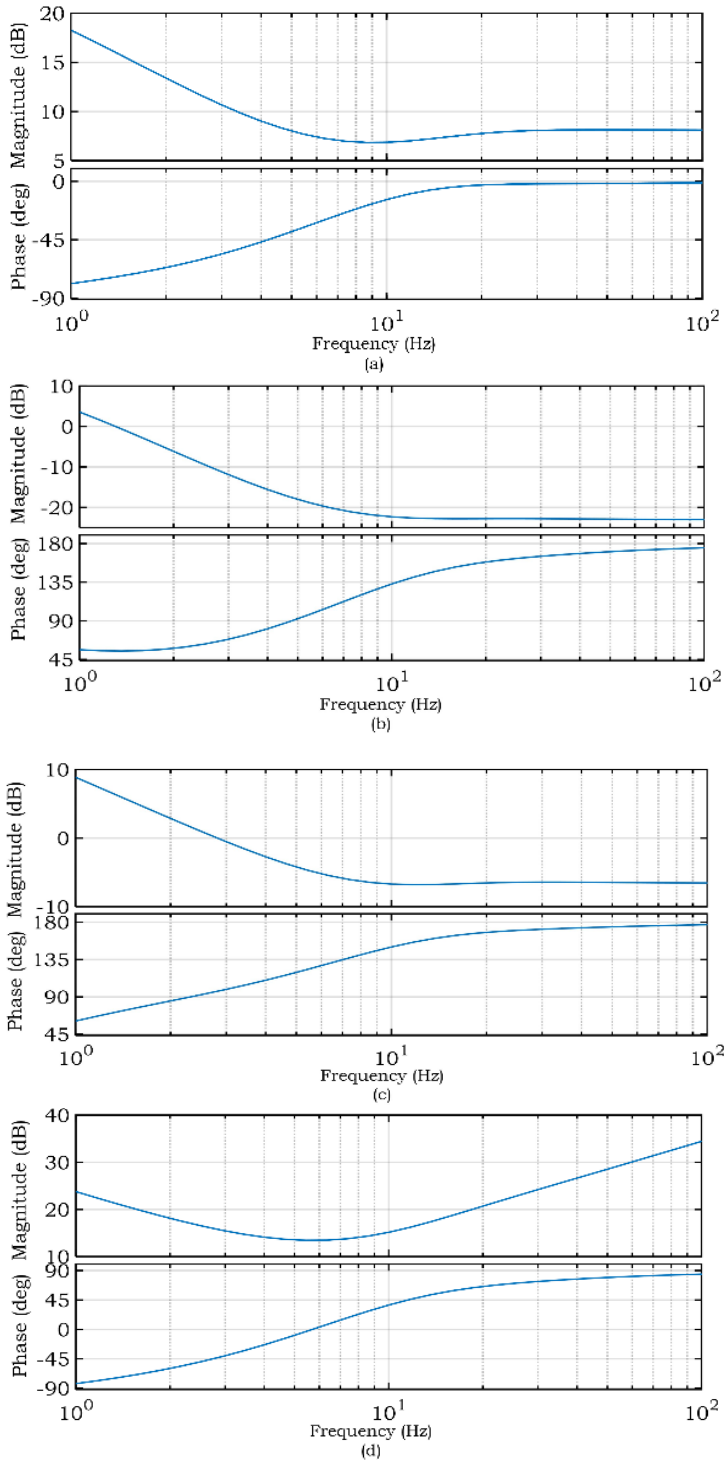

Fig. 2-13. Bode plots of the equivalent impedance of the HVDC-SEC (a) Z_{dd} (b) Z_{dq} (c) Z_{qd} (d) Z_{qq}, when the HVDC-SEC controls V_{PCC}.

Fig. 2-13 shows that;1) Z_{dq} and Z_{qd} is inductive at all sub-synchronous frequencies, 2) Z_{dd} is capacitive at all sub-synchronous frequencies 3) Z_{qq} is capacitive when frequencies are below 6 Hz and becomes inductive when the frequency is higher than 6 Hz. Therefore, HVDC-SEC with only V_{PCC} control strategy has an inductive or capacitive property which might interact with WF based on type 3 and 4 WTGs.

Similar conclusions can be drawn when comparing Figs. 2-12 and 2-13. The HVDC-SEC has an inductive or capacitive property which might interact with WF based on type 3 and 4 WTGs.

2.3.3 The effect of system parameters on SSR oscillations in WFs with HVDC connection

As discussed in [28-30], the WF output power, control schemes and control parameters of both GSC of WTG and SEC of HVDC transmission system have a significant effect on the SSR oscillation in the system as summarized in Table 2-5.

Table 2-5. SSR Influence Factors in WF with HVDC transmission system [28-30].

System variables		Influence
Line impedance between WF and VSC-HVDC		Large impedance causes resonance [30].
WF parameters	WF output power	Large WF output power leads to resonance [29, 30].
	GSC current controller	P term provides positive damping [28, 30]. I term has less impact [28, 30].
	GSC V_{DC} controller	P term provides negative damping [28, 30].
HVDC	Control scheme	The circulating current control in MMC makes HVDC less vulnerable to interact with WF [29].
	SEC current controller	P term provides positive damping [28, 30].
	SEC *V*PCC controller	P term provides positive damping [[28, 30].

2.3.4 Existing mitigation methods for WFs with HVDC connection

First, the SSR oscillations can be mitigated by reshaping system impedance. To achieve this objective, in [28], the controller bandwidth has been controlled. In [29], authors adopt the virtual control method, which is similar to the paralleled-connect virtual impedance method, which would be discussed in Chapter 3 in detail, to provide additional damping. In [38], the impedance of SEC is regulated by adding resonant compensation blocks. This method is essentially the virtual

impedance method, which can be derived by replacing the LPF blocks in Fig. 2-7 with a band-pass filter (BPF). The BPF blocks are used to choose SSR signals at specific frequencies. This method may have better SSR damping performance if the SSR oscillation frequencies are known in advance. However, in practical applications, the SSR frequencies are changing with system parameters. Therefore, this method may not be very effective to damp SSR oscillations in practice.

2.4 Summary

In this chapter, the mechanisms, impact factors and existing SSR damping schemes in WFs based on type 3 WTGs, WFs based on type 4 WTGs and WFs with HVDC connection are thoroughly investigated. The impedance model-based analysis method is employed during the study.

First, the essential root cause of the SSR issue in WFs is the negative equivalent resistance. The negative resistance is caused by the slip in type 3 WTGs and is due to the control systems of GSC in type 4 WTGs. For an interconnected system with WFs and HVDC transmission systems, the SEC of the HVDC also has a negative equivalent resistance. Therefore, all these systems have a potential to suffer the SSR oscillations.

Second, the different impedance properties of WFs, whether inductive (type 3 WTG-based WFs) or capacitive (type 4 WTG-based WFs), dominate the external triggers for SSR oscillations. That is for type 3 WTGs the external cause is series compensation networks, and for type 4 WTGs it is weak grids. HVDC transmission system interacts with WFs based on both type 3 and 4 WTGs since it has either inductive or capacitive impedance characteristics in the different frequency. Moreover, the PLL block in the GSC could potentially cause multiple SSR frequencies problem.

Chapter 3
Proposed Improved SSR Mitigation Methods

In this chapter, the improved SSR mitigation methods are studied. First the SSR damping schemes in WFs based on Type 3 WTGs are investigated, following by the mitigation methods in type 4 WTGs. At last, the problem brought by the traditional PLL block is discussed and advanced PLL technologies are employed to eliminate SSR oscillations. The performance of the enhanced SSR mitigation methods are validated using simulations in both frequency- and time-domains.

3.1 Mitigation schemes in WFs based on type 3 WTGs

As discussed in Chapter 2, two most representative SSR mitigation methods in WFs based on type 3 WTGs are; 1) GSC with virtual impedance control, and 2) STATCOM with SSRDC. In this section, these two methods will be thoroughly analyzed and compared. And the improved methods are proposed to realize a better SSR damping performance.

3.1.1 Virtual impedance scheme

As shown in Fig. 2-7, the integrated virtual impedance is integrated in the GSC branch using the series-connected virtual impedance control [37]. However, regulating the system impedance via controlling that of the GSC is difficult. Because it has higher equivalent impedance compared to the RSC and RSC and GSC branches are connected in parallel. The total equivalent impedance of the system is determined by the RSC branch. Therefore, active GSC control does not provide SSR damping at the desired level using existing virtual impedance control. Alternatively, the virtual impedance can be connected in parallel with GSC. The modification regulates the overall impedance of the system. This concept has been presented in [37] without a detail analysis and validation. Therefore, it is further investigated in this section. Corresponding impedance model under this control scheme is shown in Fig. 3-1.

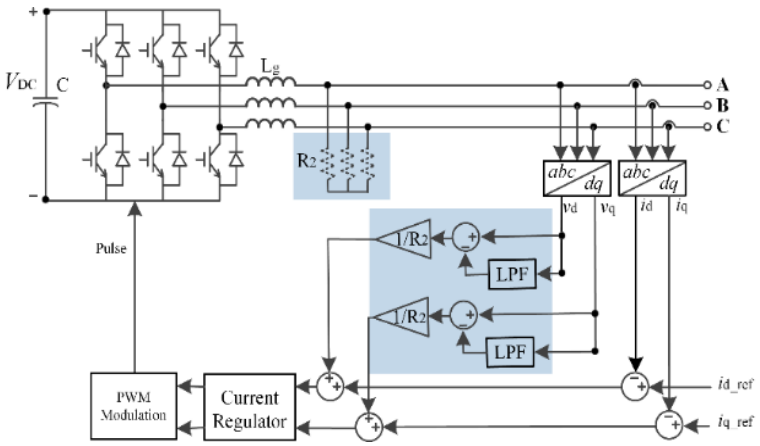

Fig. 3-1. Configuration of GSC with parallel-connected virtual impedance control.

The equivalent impedance ($Z_{G\_withdamping}$) when there is a series-connected virtual impedance in each GSC branch can be obtained based on (2-4), as in (3-1).

$$Z_{G\_withdamping} = Z_{GSC} + Z_{Lg} + R_1 \tag{3-1}$$

The total equivalent impedance of the WTG with additional series-connected virtual impedances can be obtained as in (3-2) via (2-6) and (3-1).

$$Z_{DFIG\_series} = (Z_{SR} // Z_{G\_withdamping}) / n \tag{3-2}$$

The equivalent impedance of the system with parallel-connected virtual impedance is shown in Fig. 3-1. The total equivalent impedance of the WTG with the parallel-connected virtual impedance is given by (3-3).

$$Z_{DFIG\_parallel} = (Z_{SR} // Z_G // R_2) / n \tag{3-3}$$

The real part of the total equivalent impedance as a function of frequency is plotted in Fig. 3-2 based on (3-2) and (3-3). When compared to the generator resistance shown in Fig. 2-3(b), whether the added series-connected virtual impedance or parallel-connected virtual impedance is capable to greatly increase the equivalent resistance of the WTG to compensate the negative resistance at the all desired frequencies to damp SSR oscillations. The parallel-connected virtual impedance control has better impedance property than the series-connected method. However, the available

power rating of the WF becomes a concern in practical applications as impedances are added in parallel with the system requires higher damping current.

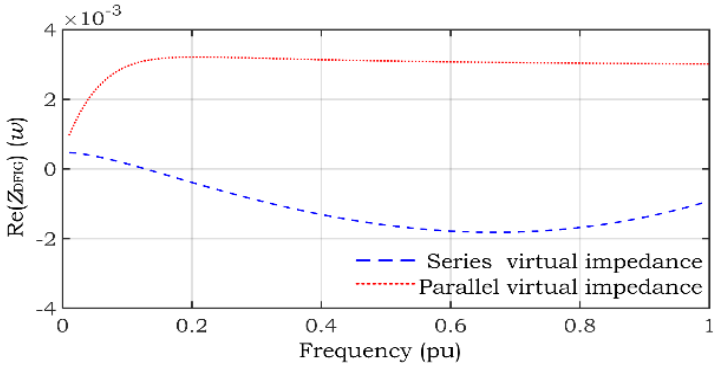

Fig. 3-2. Real part of equivalent impedance of type 3 WTG
with series-connected (dashed line), and with parallel-connected (dotted line) virtual impedance control.

In summary, there are some limitations behind preventing SSR oscillations using series- and parallel-connected virtual impedances in practical applications, although they improve the impedance characteristics of the system. For example, series-connected virtual impedance cannot provide the required damping in IG based system since the overall impedance is determined by the RSC branch. On the other hand, the potential overcurrent caused by parallel virtual impedance makes this approach not very practical.

3.1.2 STATCOM with SSRDC scheme

Effectiveness of the STATCOM to mitigate SSR damping is investigated to find a suitable SSR damping strategy. First, the impedance model of the STATCOMs under the reactive power and PCC voltage control modes have been studied. Besides that, impedance characteristics of a system based on the STATCOM and SSRDC are also investigated.

1) Impedance Properties of a STATCOM

Impedance model of a STATCOM is derived using the impedance model of a VSC provided in [53,54]. The *d*-axis reference signal of the inner current loop (i_{d_ref}) is obtained considering the DC-link voltage (V_{DC}) control while obtaining the *q*-axis reference signal (i_{q_ref}) using either by PCC voltage (V_{PCC}) control or reactive power (Q) control. As STATCOM is also a voltage source

converter (VSC) like GSC in type 4 WTGs, the impedance model of STATCOM can be obtained using Figs. 2-9(b), (c) and (d).

Fig. 3-3 shows the real part of the impedances Z_{dd}, Z_{dq}, Z_{qd} and Z_{qq}, defined in (2-8) when the q-axis of STATCOM adopts V_{PCC} control and Q control. The impedance is calculated based on per unit value of the sub-synchronous frequencies by selecting 60 Hz as the base frequency.

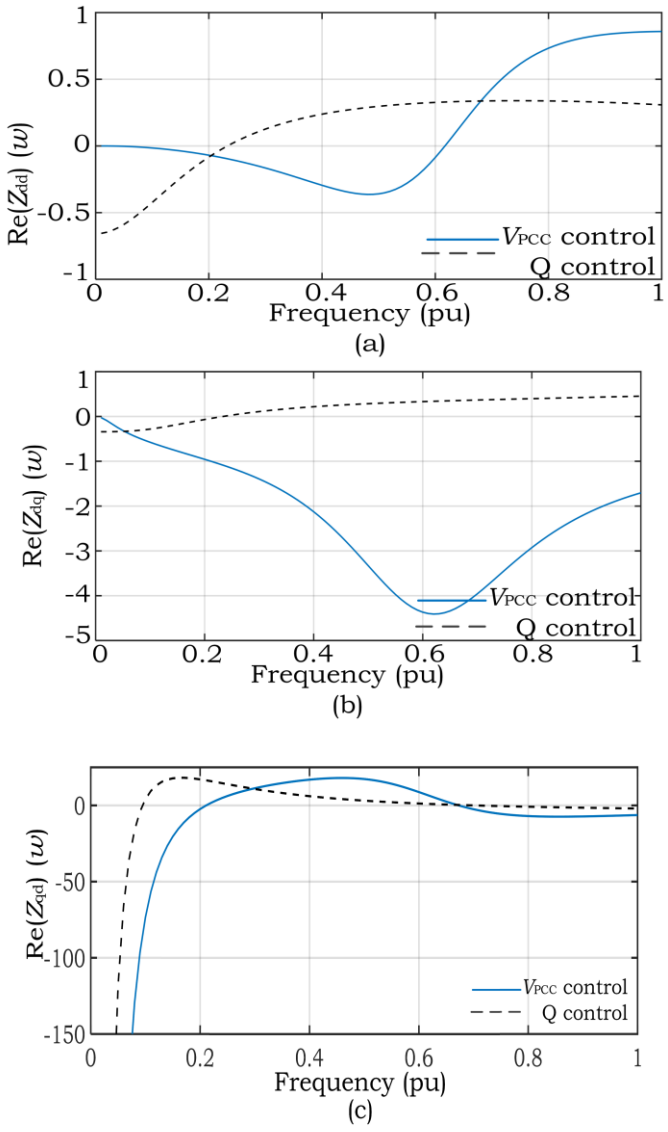

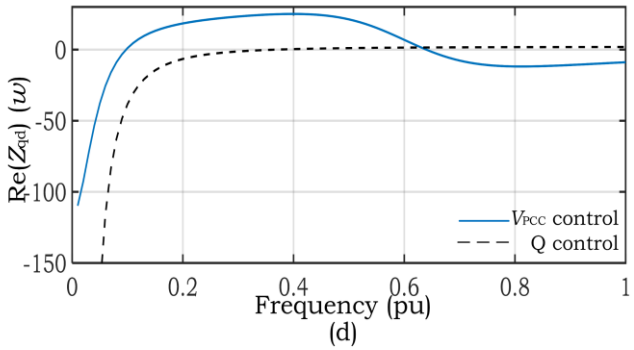

Fig. 3-3. Real part of equivalent impedance of STATCOM with V_{PCC} control, and Q control (a) Z_{dd} (b) Z_{dq} (c) Z_{qd} (d) Z_{qq}.

The resistance Z_{dd} and Z_{dq} greatly increase in Q control mode and the change in control strategies have less impact on Z_{qd} and Z_{qq}. STATCOM may provide negative damping to SSR oscillations as the real parts of impedance Z_{dd} and Z_{dq} (resistances of Z_{dd} and Z_{dq}) are negative in the voltage control mode. Moreover, the resistance of Z_{dd} becomes positive when the frequency is above 0.2 p.u. (12 Hz) in the Q control mode. The resistance of Z_{dq} becomes positive when the frequency is larger than 0.03 p.u. (1.8 Hz) in the Q control mode. Besides, the resistance of Z_{qd} and Z_{qq} becomes negative when the frequency is higher than about 0.6 p.u. (36Hz) under voltage control, decreasing the damping to SSR oscillations.

The overall performance of STATCOM under Q control mode is much better than that under V_{PCC} control mode. Hence, STATCOM is suggested to be operated the in Q control mode rather than V_{PCC} control mode to obtain positive SSR damping.

2) Impedance properties of a STATCOM with SSRDC

In the existing studies, the generated SSR damping signal shown in Fig. 2-4 is usually fed into the q-axis of the STATCOM control loop, as shown in Fig. 2-5. Therefore, small incremental change in the q-axis reference signal of the inner current loop is given by (3-4) and it is obtained by adding damping signal to (2-13); where G(s) is the transfer function of the SSRDC, which can be obtained using Fig. 2-4.

$$\Delta i_q^{ref} = F_1'\Delta v_{gd} + F_2'\Delta v_{gq} + G(s)\Delta v_{gq} \tag{3-4}$$

The SSRDC transfer is simplified approximating band-pass filter (BPF) characteristics $G(s) = k\dfrac{2\xi\omega_s s}{s^2 + 2\xi\omega_s s + \omega_c^2}$.

However, the SSR damping signal is fed into the *d*-axis of the STATCOM control loop to improve the performance. Therefore, small incremental change in the *d*-axis reference signal is obtained as in (3-5) by adding damping signal to (A.1).

$$\Delta i_d^{ref} = T_1'\Delta v_{gd} + T_2'\Delta v_{gq} + G(s)\Delta v_{gd} \tag{3-5}$$

The real part of the impedance model of STATCOM when SSR damping signal fed into *q*-axis, and into both *d*- and *q*-axes is plotted in Fig. 3-4.

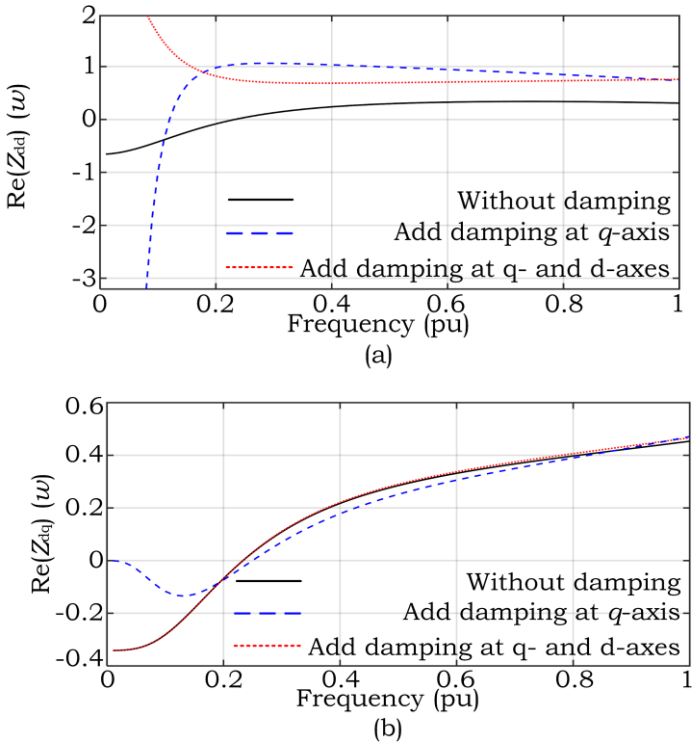

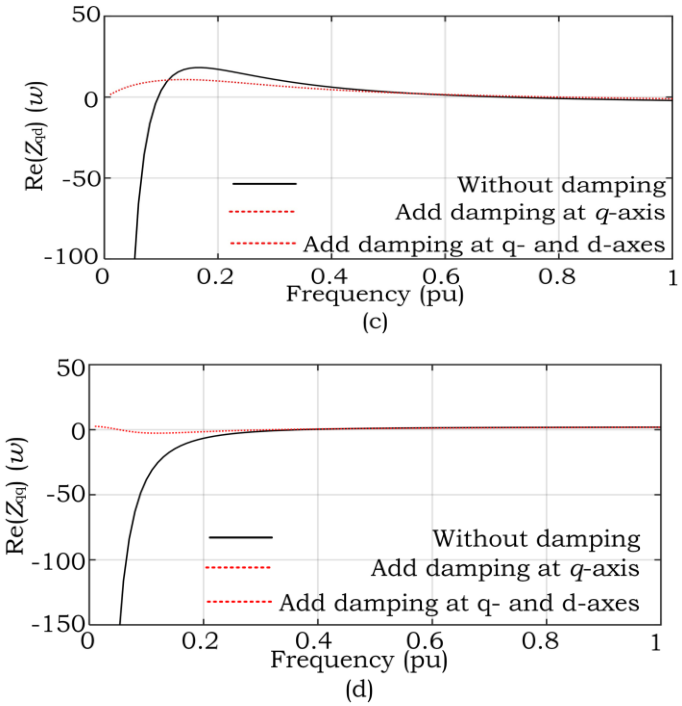

Fig. 3-4. Real part of equivalent impedance of STATCOM without additional damping, with damping at *q*-axis, with damping at both *d*- and *q*-axes (a) Z_{dd} (b) Z_{dq} (c) Z_{qd} (d) Z_{qq}.

Fig. 3-4 (a) shows that both two control strategies can provide more positive damping to the system. The system with SSRDC damping signal at both *d*- and *q*-axes outperforms the system only having the damping signal at *q*-axis at relatively low frequencies (< 12 Hz). Fig. 3-4 (b) shows that there is no significant improvement over each other in Z_{dq} at frequencies above 12 Hz. On the contrary, Figs. 3-4 (c) and (d) show that impedance characteristics of Z_{qd} and Z_{qq} can be improved at relatively low frequencies (< 5 Hz), although it is not the case when adding damping only at *q*-axis. Therefore, improved damping performance can be obtained adding control signals into both *d*- and *q*-axes.

The time-domain simulations have been performed to analyze the damping performance of adding SSRDC on both *d*- and *q*-axis of the control loop. The obtained results shown in Figs. 3-5 and 3-6 reveal that STATCOM with SSRDC is a feasible solution to damp SSR oscillations in WFs based on type 3 WTGs.

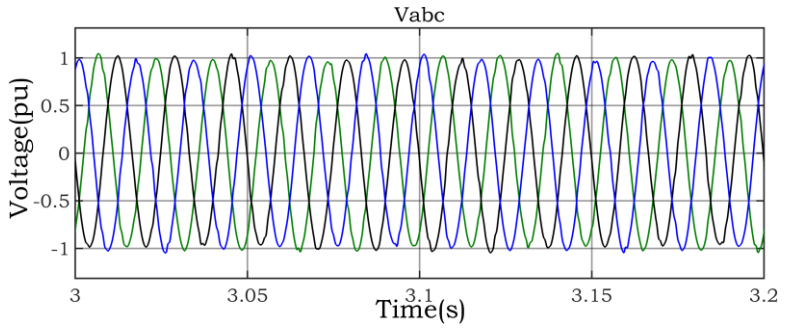

(a)

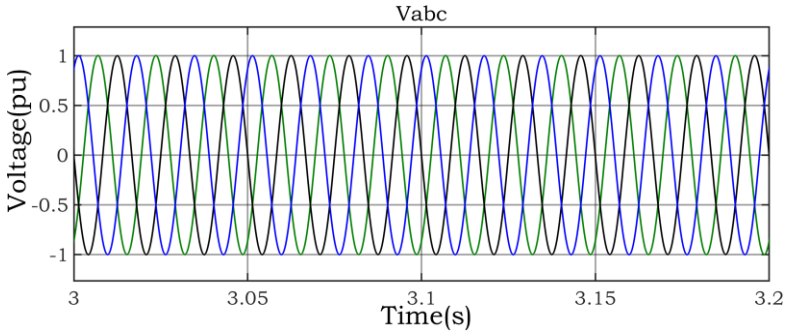

(b)

Fig. 3-5. Simulation results in the time-domain when STATCOM integrating (a) SSRDC in *q*-axis (b) SSRDC in both *d*- and *q*-axes.

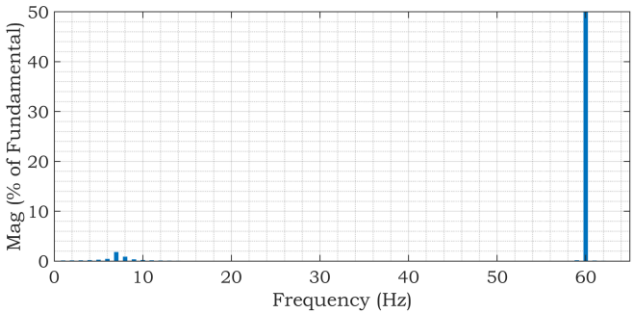

(a)

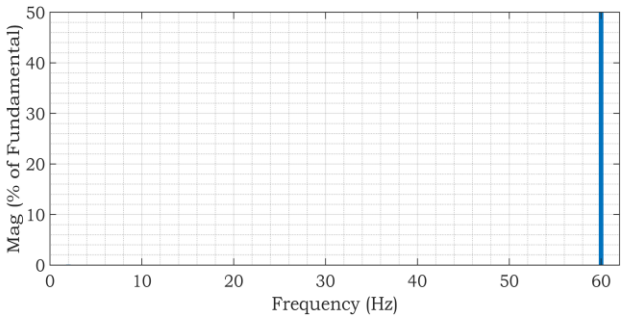

(b)

Fig. 3-6. FFT analysis results in the time-domain when STATCOM integrating (a) SSRDC in *q*-axis (b) SSRDC in both *d*- and *q*-axes.

In summary, the above analysis shows that the desirable SSR damping performance in WFs based on type 3 WTGs cannot be obtained using the power converters of the WTG via utilizing either series- or parallel-connected virtual impedance control strategy. Instead, additional FACTS devices should be employed. When using STATCOM device, the *q*-axis of the outer loop should be used to control the Q rather than V_{PCC}, and the damping signal generated by SSRDC should be fed into both *d*- and *q*-axes. In this way, desirable SSR damping performance can be obtained while providing reactive power compensation using STATCOM. However, SSR damping provides by STATCOM may not sufficient in large WFs. Therefore, STATCOM with energy storage system (ESS) is viable options that can be considered to damp SSR oscillations. As discussed in [67], STATCOM with an ESS system enables the active power control and consequently, enables the system to fix unbalanced power flow, transient and dynamic stability issues, and power oscillations.

3.2 Mitigation schemes in WFs based on type 4 WTGs

As discussed in Chapter 2, the outer control loop of GSC has an impact on SSR oscillations. Hence, an improved SSR mitigation method is developed by modifying the control strategy of the outer control loop. Typically, the vector control strategy is adopted in the full power converters of type 4 WTG. The *d*-axis determines DC-link voltage (V_{DC}) or active power (P) and the *q*-axis controls the voltage at the PCC (V_{PCC}) or reactive power (Q). The configuration of controllers in GSC is shown in Fig. 2-9. Altogether, there are four control schemes that can be adapted to control GSC: (1) V_{DC} control (*d*-axis) + V_{PCC} control (*q*-axis) (the impedance model can be build using Figs. 2-9(b) and (d)), (2) V_{DC} control (*d*-axis) + Q control (*q*-axis) (the impedance model can be build using Figs. 2-9(c) and (d)), (3) P control (*d*-axis) + V_{PCC} (*q*-axis) (the impedance model can be build using Figs. 2-9(b) and (e)), and (4) P control (*d*-axis) + Q control (*q*-axis) (the impedance model can be build using Figs. 2-9(c) and (e)).

As mentioned in Chapter 2, in the traditional control strategy, the MSC controls the power flow and the GSC stabilize the DC-link voltage. Therefore, the GSC adopts V_{DC} + V_{PCC} control. Here, the traditional control strategy and the other three control strategies are studied to find the most

suitable strategy to mitigate the SSR oscillations. A more detailed discussion about the general approach of interchanging the control objectives of the GSC and RSC of a type 4 WTG can be found in [69]. The above analysis is performed using the impedance model-based and time-domain analyses. The obtained bode plots of GSC impedance model with the four control strategies are shown in Figs. 3-7 - 3-10.

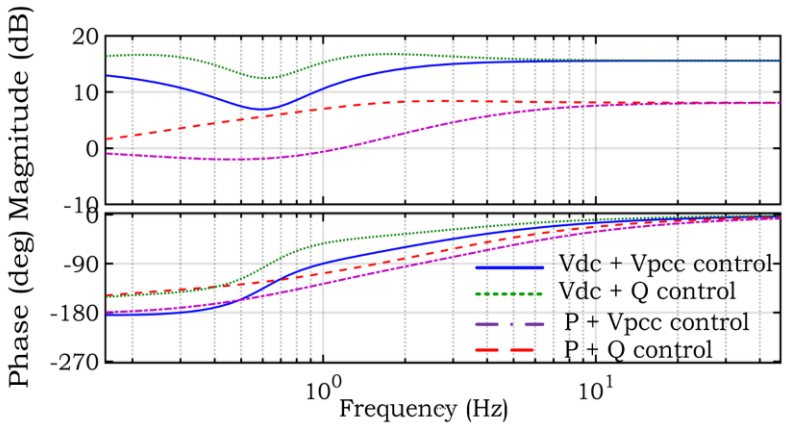

Fig. 3-7. Bode plot of Z_{dd} plot of when GSC adopting four types of control strategies.

Fig. 3-7 shows that the impedance properties of Z_{dd} with the control strategies $P + V_{PCC}$ and $P + Q$ control are similar. Their magnitudes are almost the same when the frequency is above 3 Hz. Also, the impedance properties of Z_{dd} with the control strategies $V_{DC} + V_{PCC}$ and $V_{DC} + Q$ control are similar. Hence, the impact of the control methods on the d-axis (either it is P control or V_{DC} control) is significant than that on the q-axis in shaping the impedance property of Z_{dd}. The SSR oscillation frequency is lower when adopting P control compared to the V_{DC} control. At the SSR frequencies, the phase angles of impedance models are below zero (showing a capacitive property) implying an interaction with the weak grid.

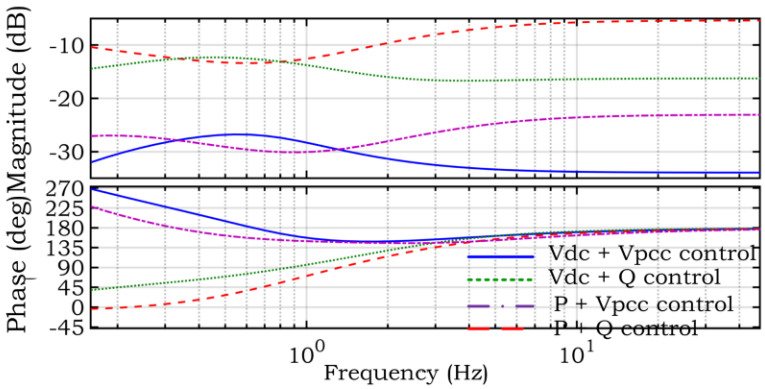

Fig. 3-8. Bode plot of Z_{dq} plot of when GSC adopting four types of control strategies.

The Bode plot of Z_{dq} in Fig. 3-8 shows that the phase angles of the four impedance models are above zero under four control strategies. So, Z_{dq} will not contribute to the SSR oscillations in a system based on type 4 WTGs and a weak grid.

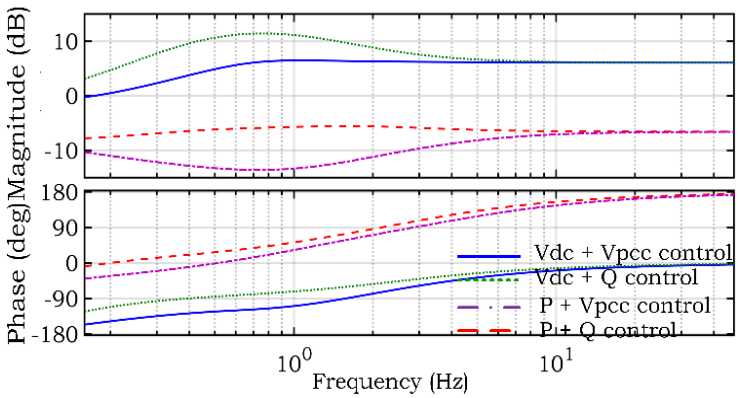

Fig. 3-9. Bode plot of Z_{qd} plot of when GSC adopting four types of control strategies.

Fig. 3-9 shows that impedance properties of Z_{qd} are similar when adopting the V_{DC} + V_{PCC} and V_{DC} + Q control schemes. The magnitudes of Z_{qd} are almost the same and the phase angles are above zero under sub-synchronous frequencies. The impedance Z_{qd} shows the same impedance properties when adopting the P + V_{PCC} and P + Q control schemes. These observations also prove that the control strategy on the d-axis (either it is P control or V_{DC} control) dominates the impedance property of Z_{qd}. The phase angle of the impedance model is above zero (showing an inductive property) under SSR frequencies when adopting P control but it is less than zero

(showing a capacitive property) when using V_{DC} control. Therefore, the impedance Z_{qd} will not interact with the weak grid under P control, and conversely, under V_{DC} control, it will. Hence, the P control would be more useful to avoid SSR oscillations under the weak grid conditions.

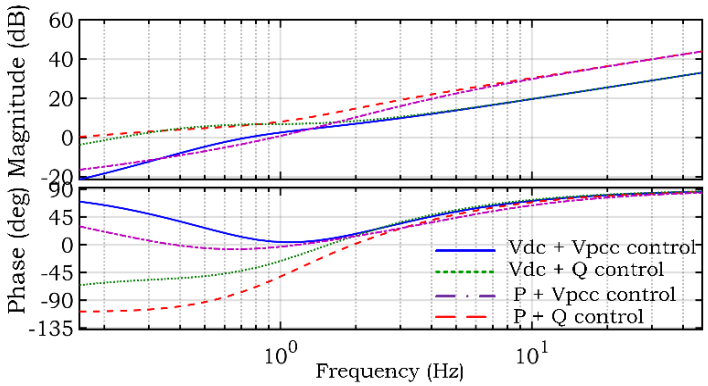

Fig. 3-10. Bode plot of Z_{qq} plot of when GSC adopting four types of control strategies.

The bode plots of Z_{qq} shown in Fig. 3-10 have a similar property under four control strategies. At sub-synchronous frequencies, the phase shift is less than zero and there is capacitive impedance property. Hence, there is a potential to interact with a weak grid.

In summary, the impedance properties of GSC are similar when adopting V_{DC} + V_{PCC} and V_{DC} + Q control schemes. A similar conclusion can be made when GSC adopts P + V_{PCC} and P + Q control schemes. Therefore, the control strategy on the d-axis (either it is P control or V_{DC} control) dominates the impedance properties of the GSC compared to the strategy based on the q-axis (either it is Q control or V_{PCC} control). And P + V_{PCC} and P + Q control schemes are better than V_{DC} + V_{PCC} and V_{DC} + Q control schemes to solve the SSR problem in type 4 WTGs with weak-grid.

The time-domain simulation results shown in Figs. 3-11 and 3-12 validate the above analysis. Figs. 3-11 and 3-12 show the waveforms of grid voltage when adopting four types of control strategies and corresponding harmonic contents of the grid voltage.

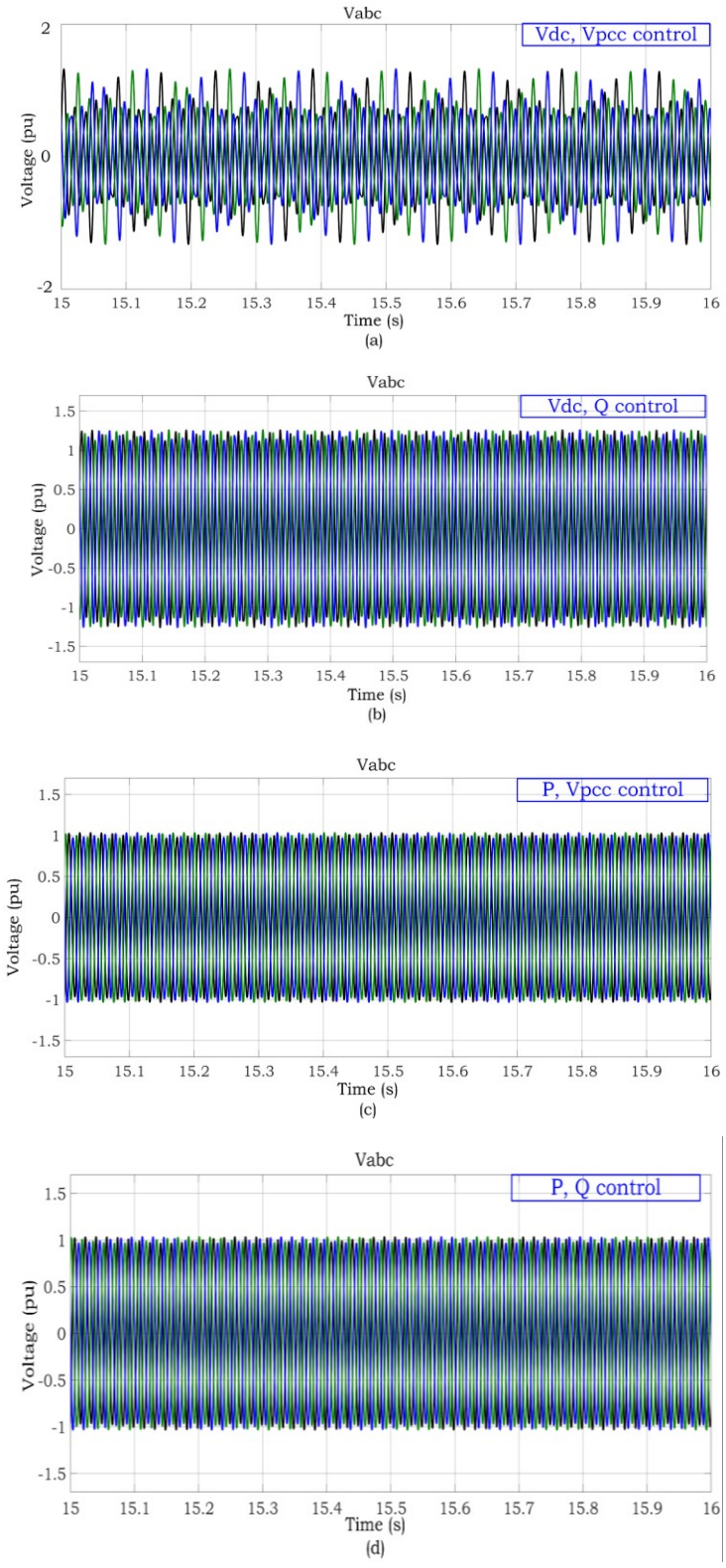

Fig. 3-11. Waveforms of grid voltage when adopting (a) V_{DC} + V_{PCC}, (b) V_{DC} + Q (c) P + V_{PCC}, and (d) P + Q control strategies.

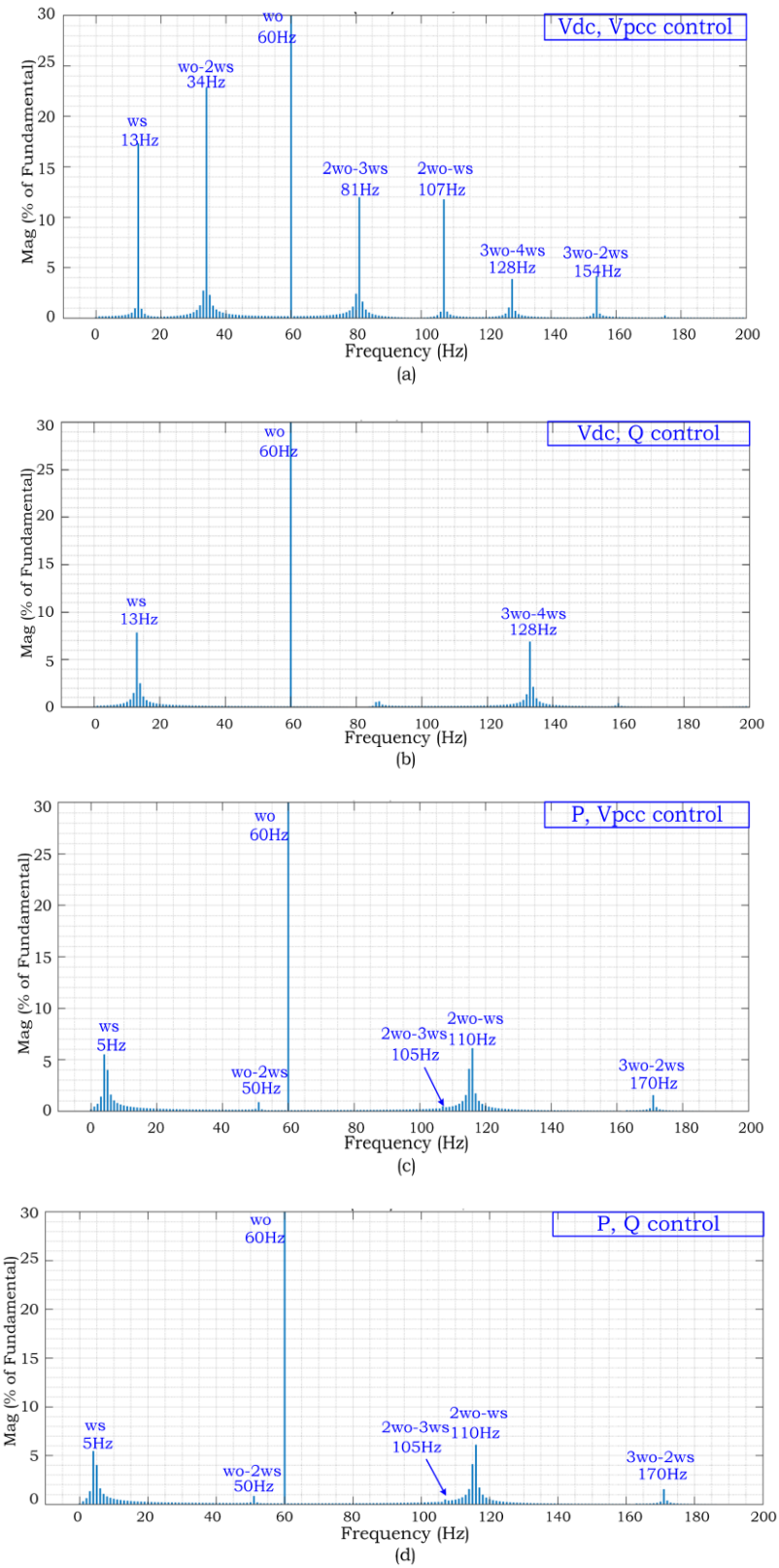

Fig. 3-12. Harmonic analysis results of grid voltage under (a) V_{DC} + V_{PCC}, (b) V_{DC} + Q (c) P + V_{PCC}, and (d) P + Q control strategies.

From Fig. 3-11 and Fig. 3-12, SSR oscillations under $V_{DC} + V_{PCC}$ control mode are more serious, compared with the other three control strategies. Figs. 12(c) and (d) shows that the SSR damping performance is similar with $P + V_{PCC}$ and $P + Q$ control strategies and it has a better performance compared to $V_{DC} + V_{PCC}$ and $V_{DC} + Q$ control schemes. Hence, the control strategy based on the *d*-axis dominates the SSR damping performance, and *P* control on the *d*-axis has a better capability to damp SSR oscillations comparing with V_{DC} control on the *d*-axis. Another important finding from fig. 3-13 is that there are multiple SSR oscillations appeared in the system at frequencies w_s, $2w_o - w_s$, $w_o - 2\,w_s$, $3\,w_o - 2w_s$. This is due to the traditional PLL block in the control system, which will be discussed in detail next in this chapter.

In conclusion, both frequency- and time-domain simulation results show that the control scheme on the *d*-axis of GSC has a significant impact on the impedance property of GSC and consequently to affect SSR damping performance. The *P* control on *d*-axis shows better SSR damping performance compared to the conventional control strategy (i.e. V_{dc} control on *d*-axis). Hence, to avoid SSR oscillations between type 4 WTGs and the weak grid, an improved alternative is let MSC could control the $V_{DC} + V_{PCC}$ and let GSC control power flow (i.e. $P + Q$ control).

The above study of the GSC of type 4 WTGs is also suitable to analyze SEC of an HVDC system and STATCOM since all of them are VSCs. The potential to appear SSR oscillations between SEC of HVDC and GSC of type 4 WTGs can also be alleviated when SEC adopts $P + Q$ control like GSC of a type 4 WTG. Second, in the traditional setup, STATCOM only provides reactive power compensation but not active power compensation. The above analysis shows that the active power control of VSC alters its impedance property. Hence, STATCOM with ESS systems has more flexibility to provide SSR damping for different WF systems than traditional STATCOM.

3.3 Advanced PLL technologies for SSR mitigation

Based on the previous study, the conventional synchronous reference frame PLL (SRF-PLL) block in type 4 WTG will give rise to multiple SSR frequencies in the system. In order to eliminate that impact caused by the SRF-PLL block, more advanced three-phase PLL technologies are studied and compared in SSR scope.

This chapter starts with the introduction of the mechanism why traditional SRF-PLL block could cause the multiple SSR frequencies issue, followed by a brief overview of modern three-phase PLL technologies. Next, some alternatives are utilized in type 4 WTGs and corresponding simulations to done to validate their performance in SSR damping. The outcome of this chapter provides practical PLL scheme in WF to handle SSR oscillations.

3.3.1 Influence of SRF-PLL block in SSR oscillations

1) Model of SRF-PLL

The diagram of the conventional SRF-PLL is shown in Fig. 3-13, in which the phase detector (PD), loop filter (LF), and voltage-controlled oscillator (VCO) are included. PD is implemented by utilizing the Park's transformation (abc / dq) to the input three-phase input signals (v_{abc}). The q-axis output of the PD, which contains phase error information, is then passed to the LF. LF is realized using the PI (proportional-integral) controller. The VCO, which is essentially a integrator, provide the estimated frequency. ω_{pll} and θ_{pll} are the frequency and phase angle estimated by the SRF-PLL, respectively; ω_o is the normal grid frequency.

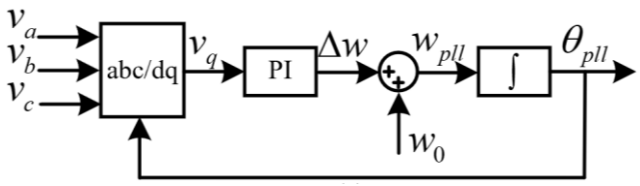

Fig. 3-13. The diagram of traditional SRF-PLL block.

The input three-phase signal can be represented as (3-6),

$$\begin{aligned} v_a(t) &= V\cos(\theta) \\ v_b(t) &= V\cos(\theta - \frac{2}{3}\pi) \\ v_c(t) &= V\cos(\theta + \frac{2}{3}\pi) \end{aligned} \tag{3-6}$$

The Park's transformation is denoted as (3-7).

$$P(\theta_{PLL})=\begin{bmatrix} \cos\left(\theta_{PLL}+\frac{\pi}{2}\right) & \cos\left(\theta_{PLL}+\frac{\pi}{2}-\frac{2\pi}{3}\right) & \cos\left(\theta_{PLL}+\frac{\pi}{2}+\frac{2\pi}{3}\right) \\ -\sin\left(\theta_{PLL}+\frac{\pi}{2}\right) & -\sin\left(\theta_{PLL}+\frac{\pi}{2}-\frac{2\pi}{3}\right) & -\sin\left(\theta_{PLL}+\frac{\pi}{2}+\frac{2\pi}{3}\right) \end{bmatrix} \tag{3-7}$$

By applying (3-7) to (3-6), the transformed signals on the *dq* reference frame can be obtained as (3-8).

$$\begin{bmatrix} v_d \\ v_q \end{bmatrix} = P(\theta_{PLL}) \begin{bmatrix} v_a \\ v_b \\ v_c \end{bmatrix} \tag{3-8}$$

where

$$\theta_{PLL} = \int \left[\omega_0 + \left(K_P + \frac{K_I}{p} \right) v_q \right] \mathrm{dt} \tag{3-9}$$

At steady state $\theta_{PLL} = \omega_0 t$.

2) Influence of SRF-PLL to SSR oscillations

As discussed in [10], the SRF-PLL will cause multiple SSR frequencies problem. This phenomenon can also be observed in Fig. 3-13, that is except for the original SSR frequency ω_s (13Hz) component, some other harmonics, including $\omega_o - 2\omega_s$ (34Hz), $2\omega_o - \omega_s$ (107Hz), $2\omega_o - 3\omega_s$ (81Hz), $3\omega_o - 2\omega_s$ (154Hz), $3\omega_o - 4\omega_s$ (128Hz), can also be observed. Next, a brief explanation of this phenomenon will be provided.

Taking the SSR component with frequency ω_s into consideration, the grid voltage v_{abc} (with dot superscript) composing both fundamental (with *f* subscript) and SSR (with *s* subscript) components can be expressed as (3-10).

$$\begin{bmatrix} v'_a \\ v'_b \\ v'_c \end{bmatrix} = \begin{bmatrix} V_f \cos(\omega_0 t + \varphi_{V_f}) + V_s \cos(\omega_s t + \varphi_{V_s}) \\ V_f \cos(\omega_0 t + \varphi_{V_f} - \frac{2\pi}{3}) + V_s \cos(\omega_s t + \varphi_{V_s} - \frac{2\pi}{3}) \\ V_f \cos(\omega_0 t + \varphi_{V_f} + \frac{2\pi}{3}) + V_s \cos(\omega_s t + \varphi_{V_s} + \frac{2\pi}{3}) \end{bmatrix} \tag{3-10}$$

Referring to (3-8), then the voltages at *d*- and *q*-axes become (3-11).

$$\begin{aligned} \begin{bmatrix} v'_d \\ v'_q \end{bmatrix} &= P(\theta_{PLL}) \begin{bmatrix} v'_a \\ v'_b \\ v'_c \end{bmatrix} \\ &= \begin{bmatrix} v_{f\_d} + v_{s\_d} \\ v_{f\_q} + v_{s\_q} \end{bmatrix} \end{aligned} \tag{3-11}$$

where v_{f_d} and v_{f_q} are constant components of voltages in *d*- and *q*-axes, respectively. And v_{s_d} are v_{s_q} resonant components in *d*- and *q*-axes. Via (3-7), (3-10) and (3-11), v_{s_d} are v_{s_q} can be obtained as (3-12).

$$\begin{cases} v_{f\_d} = 0 \\ v_{s\_d} = v_s \cos\left[(\omega_o - \omega_s) t + \varphi_{V_f} + \frac{\pi}{2} - \varphi_{V_s} \right] \\ v_{f\_q} = -v_f \\ v_{s\_q} = v_s \cos\left[(\omega_o - \omega_s) t + \varphi_{V_f} + \pi - \varphi_{V_s} \right] \end{cases} \tag{3-12}$$

As can be seen from (3-9) and Fig. 3-14, the voltage component at *q*-axis will affect the steady state output of SRF-PLL. As can be seen from (3-12), due to the SSR component in grid voltage, the signal at *q*-axis will contain $\omega_o - \omega_s$ component. Hence, the phase angle generated by SRF-PLL block will contain $\omega_o - \omega_s$ component $\Delta\theta_{pll}$. And $\Delta\theta_{pll}$ can be expressed as

$$\Delta\theta_{pll} = A\cos[(\omega_o - \omega_s)t + \varphi] \tag{3-13}$$

The above analysis demonstrates when the grid voltage contains SSR component with frequency ω_s, the phase angle output of SRF-PLL will contain harmonic component with frequency $\omega_o - \omega_s$.

In the control loop, the vector control is utilized, that is the input signal of the control block will be transformed from the *abc* reference frame to the *dq* reference frame, which is realized via the PLL block. Therefore, the control signals obtained in *d*- and *q*-axes will be influenced. That is

$$\begin{bmatrix} v_d'' \\ v_q'' \end{bmatrix} = P\left(\theta_{PLL}'\right)\begin{bmatrix} v_a' \\ v_b' \\ v_c' \end{bmatrix} = \begin{bmatrix} v_{f\_d} + v_{s\_d} + v_{s\_d}' + \Delta v_{2d} \\ v_{f\_q} + v_{s\_q} + v_{s\_q}' + \Delta v_{2q} \end{bmatrix} \tag{3-14}$$

where v_{s_d}', Δv_{2d}, v_{s_q}', Δv_{2q} are new harmonics considering the output of PLL with $\omega_o - \omega_s$ component. As explained in [59], the Δv_{2q} will contain both DC and 2($\omega_o - \omega_s$) components. The DC component does not impact the steady state of the output of PLL block. However, the resonant component on the *q*-axis will once again influence the output of PLL, making 2($\omega_o - \omega_s$) components appear in the output. Therefore, due to the SSR component in grid voltage, the output of SRF-PLL will include $\omega_o - \omega_s$ and 2($\omega_o - \omega_s$) components.

To obtain the phase reference voltages, the Park's inverse transformation, i.e. (3-15), needs to be utilized to transform the voltage references in *d*- and *q*-axes to *abc* reference frame.

$$\begin{bmatrix} v_a \\ v_b \\ v_c \end{bmatrix} = P^{-1}\left(\theta_{PLL}''\right)\begin{bmatrix} v_d \\ v_q \end{bmatrix} \tag{3-15}$$

For one phase, the voltage reference becomes as (3-16) [61].

$$\begin{aligned} v_{a\_ref} = {} & A_{1a}\cos(\omega_s t + \varphi_{A_{1a}}) + A_{2a}\cos\left[\left(2\omega_o - \omega_s\right)t + \varphi_{A_{2a}}\right] + \\ & A_{3a}\cos\left[\left(\omega_o - 2\omega_s\right)t + \varphi_{A_{3a}}\right] + A_{4a}\cos\left[\left(3\omega_o - 2\omega_s\right)t + \varphi_{A_{4a}}\right] \end{aligned} \tag{3-16}$$

We can see the phase voltage now contains ω_s, $\omega_o - 2\omega_s$, $2\omega_o - \omega_s$, $3\omega_o - 2\omega_s$ components. And these components can also influence the SRF-PLL block. Finally, the phase voltage could

contain contains ω_s , $\omega_o - 2\omega_s$, $2\omega_o - \omega_s$, $3\omega_o - 2\omega_s$, $2\omega_o - 3\omega_s$, $4\omega_o - 3\omega_s$, $3\omega_o - 4\omega_s$ … components.

The above analysis displays the mechanism why SSR component could lead to multiple harmonics in the system. Next, the investigations are focused on how to improve the SSR damping performance through utilizing more advanced PLL technologies.

3.3.2 Advanced three-phase PLL technologies

As the output of traditional SRF-PLL may be polluted due to the utility distortions [71], in recent years, more and more advanced PLLs have been designed with the aim of enhancing the disturbance rejection capability of SRF-PLL. Essentially, these advanced PLL technologies are developed based on traditional SRF-PLL, integrated with additional harmonic filters. These harmonic filters can be divided into two types [72-73]:

1) overall harmonic detection, which only eliminates the fundamental component and outputs the rest harmonic content;

2) selective harmonic detection, which filters individual selective harmonics.

From the real-world examples shown in Chapter 2, for different system worldwide, the observed SSR frequencies are different. Besides that, the SSR frequencies would be affected by many factors. Therefore, we can infer the PLL technologies based on selective cancellation or extraction of harmonics may not be suitable to eliminate the SSR problem, as the SSR frequencies would change because of many factors. Therefore, the overall harmonic detection technology is more suitable to enhance the traditional SRF-PLL, in order to eliminate SSR oscillations.

As depicted in [72], the overall harmonic detection can be realized by different ways in different reference framework. That is, 1) in stationary *abc* reference framework, by using Notch Filters or Fourier based filters to only remove the fundamental component; 2) in synchronous *dq* reference framework, by using High-Pass Filter (HPF) that eliminates the dc-component; 3) by using the instantaneous power theory [74] to filter out the fundamental component by HPF.

The representative advanced PLLs based on additional harmonics filtering technologies include moving average filter-based PLLs (MAF-PLL) [75-77], notch filter-based PLLs (NF-PLL) [78], multiple synchronous reference frame-based PLLs (MSRF-PLL) [79], Complex-coefficient filter-

based PLLs (CCF-PLL) [80], delayed signal cancellation-based PLLs (DSC-PLL) [81-83], dual second-order generalized integrator-based PLL (DSOGI-PLL) [84-86]. Among the above PLL technologies, the NF-PLL, CCF-PLL, MSRF-PLL and DSC-PLL utilize the selective harmonics cancellation technologies, which may not be suitable for SSR mitigation scenario. The MAF-PLL and SOGI-PLL utilize the overall harmonic detection technology. Therefore, next the MAF-PLL and SOGI-PLL are studied in detail and employed to solve the multiple SSR frequencies problem brought by traditional SRF-PLL.

1) Moving average filter-based PLLs (MAF-PLL)

Fig. 3-14 shows the configuration diagram of MAF-PLL [75]. It enhanced the SRF-PLL with the filtering block (MAF), installed between the PD and LF, which performs as an ideal low-pass filter (LFP) to eliminate harmonics in the v_d and v_q. Essentially, MAF belongs to the second overall harmonic detection technologies, that is MAF removes the harmonics in the *dq* reference framework, only the dc-component would be left after the MAF block.

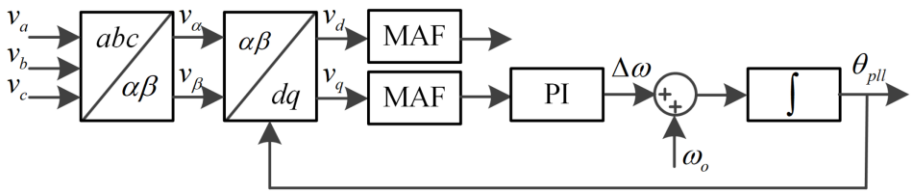

Fig. 3-14. The configuration diagram of MAF-PLL [75].

By applying the MAF block to an input signal $x(t)$, then the output becomes

$$\bar{x}(t) = \frac{1}{T_w}\int_{t-T_w}^{t} x(\tau)d\tau \tag{3-17}$$

where T_w denotes the MAF window length. As can be seen from (3-17), the MAF provides the mean value of the input signal in the time period from t-T_w to t.

Based on (3-17), the transfer function of MAF in frequency domain can be obtained as (3-18). And corresponding realization of MAF in discrete-time is shown in Fig. 3-15.

$$G_{MAF}(s) = \frac{1 - e^{-T_w s}}{T_w s} \tag{3-18}$$

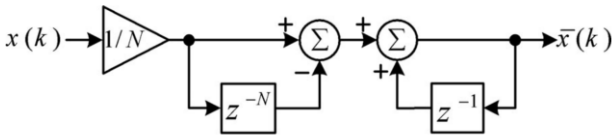

Fig. 3-15. Discrete-time realization of MAF [73].

where, N is an integer, determining the MAF order ($T_w = NT_s$, T_s is the sampling time). As can be seen from (3-17) and Fig. 3-16, the MAF requires a time equal to its window length to reach the steady-state. Hence, the wider the window length is, the slower the MAF transient response becomes. That is for a large window in MAF will cause large delay time and undesirable dynamics. Hence, the selection of the window length of the MAF is an issue of high performance, and it should be done by taking the possible resonances into consideration. By now, some advanced MAF-PLL are investigated to improve its dynamic performance, realized by integrating a phase-lead compensator [76], or a proportional component block [77] into MAF-PLL.

Considering the scenario to eliminate SSR harmonics, when the input of SRF-PLL contains ω_s component, the d- and q-axes could contain $\omega_o - \omega_s$ component after Park's transform. It can also be inferred from (3-17) when the input signal contains sinusoidal components with frequency of k * f_w (k is an integer and f_w is the equivalent frequency of MAF, i.e. $f_w = 1 / T_w$), then the output signal will be free of these oscillations. Combining these two properties together, in the SSR application scenario, the frequency of MAF can be set to 1Hz, then the harmonics (n * 1 Hz, where n is an integer) can be filtered out, which will be tested later.

2) Dual Second-order generalized integrator-based PLL (DSOGI-PLL)

SOGI technique can be an alternative of Clark's transformation to generate orthogonal signals and then be used for grid synchronization. It can perform resonant filtering at the fundamental frequency. The basic configuration of SOGI is shown as Fig. 3-16. Two integral blocks are utilized to realize the interference resistance with output signals $\Delta v_{g\alpha}$ and $\Delta v_{g\beta}$. These two output signals

are shifted by 90 degrees against each other. The transfer functions of SOGI on the D- and Q-axis are

$$D(s) = \frac{\Delta v_{g\alpha}}{v_g} = \frac{k\Delta w s}{s^2 + k\Delta w s + (\Delta w)^2} \tag{3-19}$$

$$Q(s) = \frac{\Delta v_{g\beta}}{v_g} = \frac{k(\Delta w)^2}{s^2 + k\Delta w s + (\Delta w)^2} \tag{3-20}$$

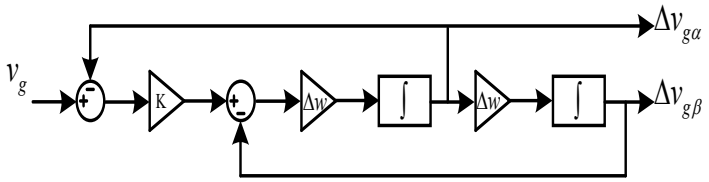

Fig. 3-16. The configuration diagram of SOGI [84].

The SOGI block can be utilized for the extraction of fundamental frequency component before SRF-PLL input as shown in Fig. 3-18. As shown in Fig. 3-17, two SOGI blocks are used to extract the filtered direct and quadrature versions of v_α and v_β. Then the fundamental frequency component can be calculated based on instantaneous symmetrical component method. This type of PLL structure is often called the Dual SOGI-PLL (DSOGI-PLL). It is widely used for grid synchronization in three-phase grid-connected power converters [86]. DSOGI-PLL has excellent dynamic performance and can effectively suppress noise, and it is easy to be implemented.

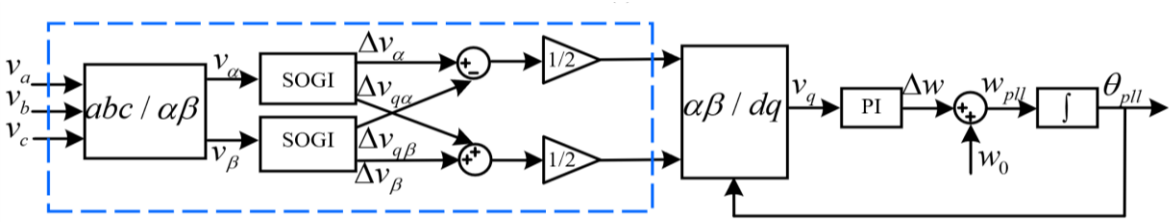

Fig. 3-17. Configuration of DSOGI-PLL block [86].

3.3.3 Advanced PLL technologies in SSR damping

As discussed previously, the grid voltage containing SSR components will cause multiple sub-synchronous frequencies problem when fed into the traditional SRF-PLL block. The advanced PLL technologies based on filtering harmonics with unknown frequencies could be alternatives in SSR damping. In this section, two advanced PLL technologies, i.e. the MAF-PLL and DSOGI-PLL, are utilized to improve the PLL performance when facing SSR oscillations. Relevant simulations are provided to validate their effectiveness in SSR mitigation.

The simulation model used in this section is similar to the simulation model used in Section 3.2. The configuration of GSC in type 4 WTGs is shown in Fig. 2-8(b). The traditional SRF-PLL shown in Fig. 2-8(b) will be replaced with two advanced PLLs, i.e. MAF-PLL and DSOGI-PLL. The overall control system of GSC is shown in Fig 2-9. In the following simulations, the GSC adopts the traditional V_{PCC} + V_{DC} control scheme. That is the control system of GSC can be built using Figs. 2-9 (b) and (d). Therefore, the effectiveness and validity of MAF-PLL and DSOGI-PLL in eliminating SSR oscillations can be evaluated by comparing with the SSR damping performance of GSC with traditional SRF-PLL employing the traditional V_{PCC} + V_{DC} control scheme and the SSR damping performance with the simulation results of GSC with SRF-PLL employing V_{PCC} + V_{DC} control scheme, which is shown in Fig. 3-11(a).

1) Simulation of MAF-PLL in SSR damping

First the model of MAF is built according to (3-18). Simulations are done to test the validity of this model. The input signal contains resonance component with frequency 47Hz ($\omega_o - \omega_s$). The signal before and after the MAF block is shown as Fig. 3-18.

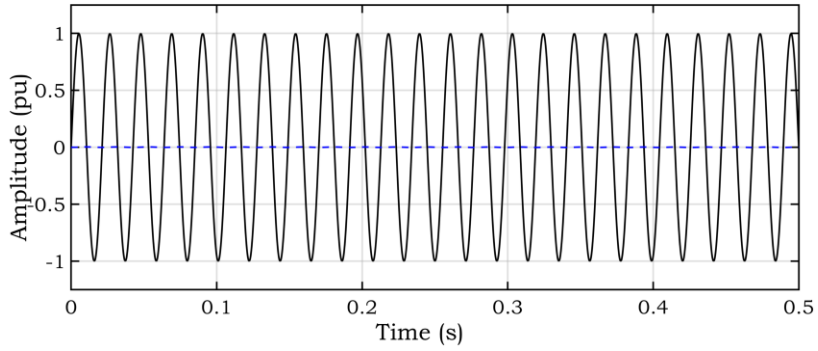

Fig. 3-18. The input signal (solid line) and output signal (dashed line) of MAF-PLL.

As can be seen from Fig. 3-18, the sub-synchronous component can be phased out by the MAF block. Next, time domains simulations to done to test the performance of MAF-PLL in SSR mitigation. The waveform of grid voltage, after using MAF-PLL, is shown Fig. 3-19(a), and corresponding harmonics analysis results are shown in Fig. 3-19(b).

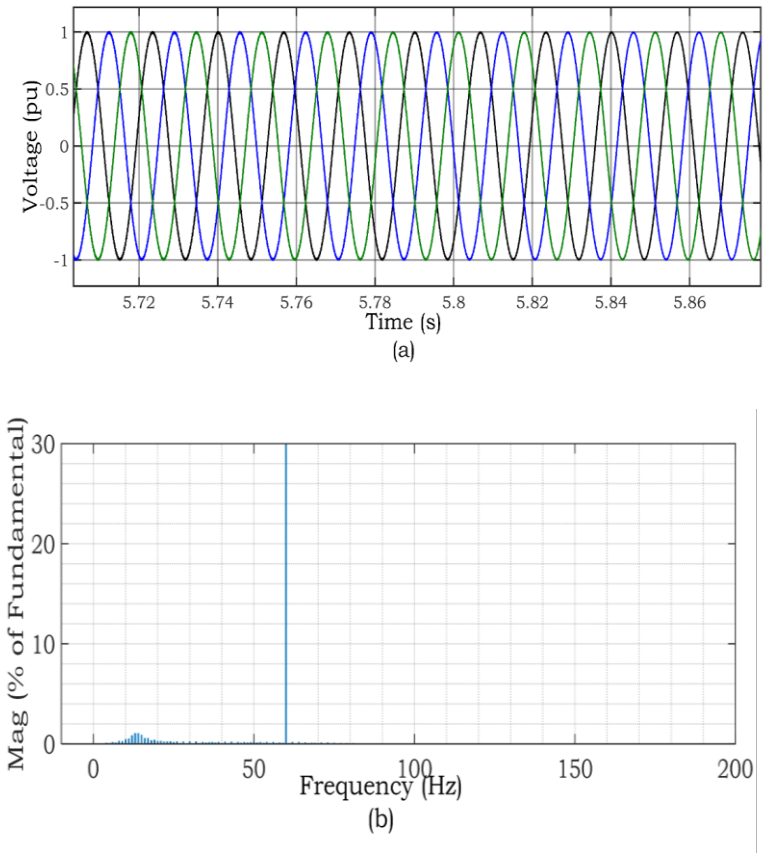

Fig. 3-19. Time domain simulation results after using MAF-PLL,
(a) grid voltage waveform, (b) harmonics analysis result.

Comparing the Fig. 3-11(a) with Fig. 3-18, we can see the sub-synchronous components are greatly reduced. A quite admiring SSR mitigation performance can be achieved by using MAF-PLL to take place of traditional SRF-PLL block.

2) Simulation of DSOGI-PLL in SSR mitigation

First, according to (3-19) and (3-20), the basic SOGI model is built. Bode plots of transfer function (3-19) and (3-20) are drawn to check the attribute of SOGI in frequency domain, shown in Fig. 3-20. The fundamental frequency is set to be 60 Hz.

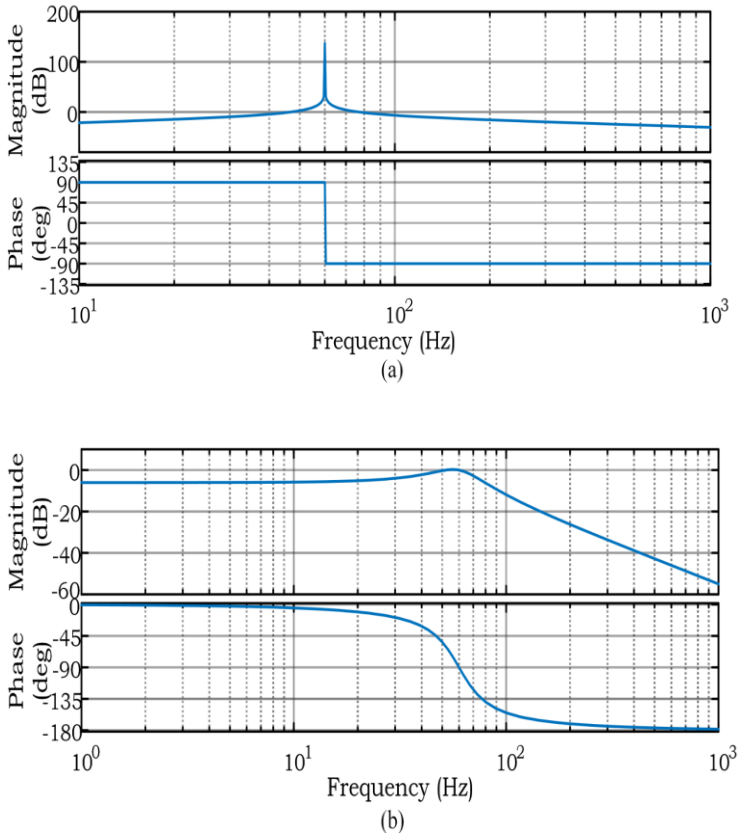

Fig. 3-20. Bode plots of transfer function of SOGI in *D*- and *Q*-axes, (a) *D*(s), (b) *Q*(s).

From Fig. 3-20, we can see the SOGI is able to generate two quadrature signals and can achieve an admiring frequency selection performance. Next, we enhance the traditional SRF-PLL with Dual SOGI blocks shown as Fig. 3-17. The transfer function of SRF-PLL and DSOGI-PLL are shown as follows

$$H_{PLL}(s)=\frac{\theta_{out}}{\theta_{in}}=\frac{K_D\times F(s)/s}{1+K_D\times F(s)/s} \tag{3-21}$$

$$H_{SOGI-PLL}(s)=\frac{\theta_{out}}{\theta_{in}}=\frac{G_\tau(s)\times K_D\times F(s)/s}{1+G_\tau(s)\times K_D\times F(s)/s} \tag{3-22}$$

where $F(s)$ is the transfer function of PI block, $F(s) = K_p + K_i / s$. Then the small signal model of SRF-PLL and DSOGI-PLL can be obtained as Fig. 3-21.

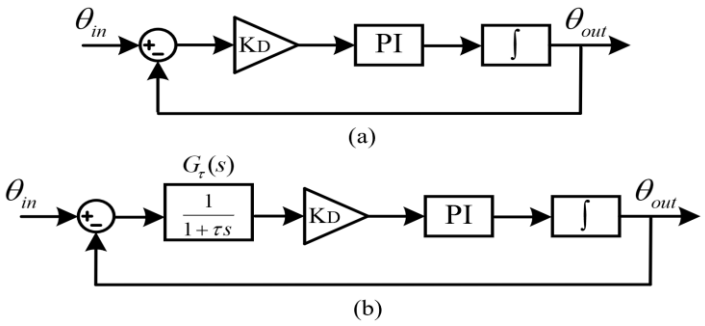

Fig.3-21. Small signal model of (a) SRF-PLL block, (b) DSOGI-PLL block.

According to the model shown in Fig. 3-21, the bode plots of SRF-PLL and DSOGI-PLL can be obtained shown in Fig. 3-22.

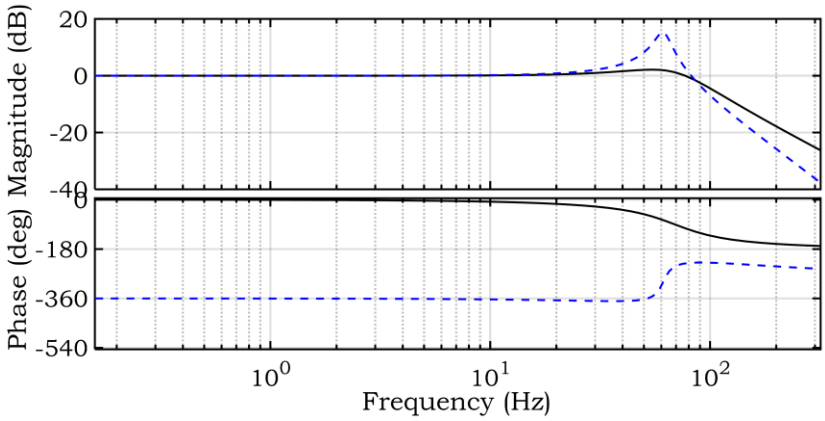

Fig. 3-22. The bode plots of small signal model of SRF-PLL (solid line) and DSOGI-PLL (dashed line).

As can be seen from Fig. 3-22, comparing with SRF-PLL, the DSOGI-PLL has a better fundamental frequency selection property. Next, simulations in the time domain are conducted to check the performance of DSOGI-PLL block. The waveform of grid voltage after using DSOGI-

PLL is shown in Fig. 3-23 (a), and corresponding harmonics analysis results are shown in Fig. 3-3-23(b).

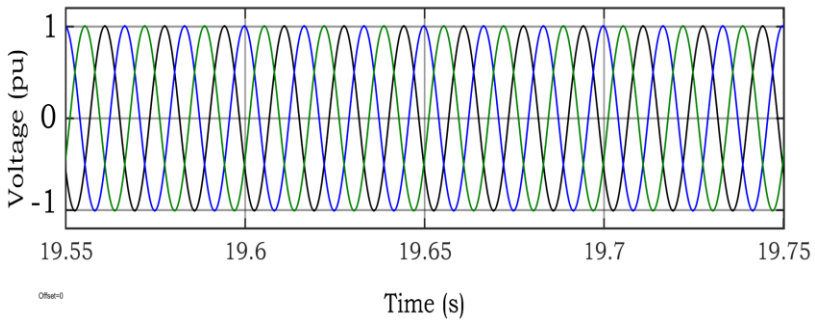

(a)

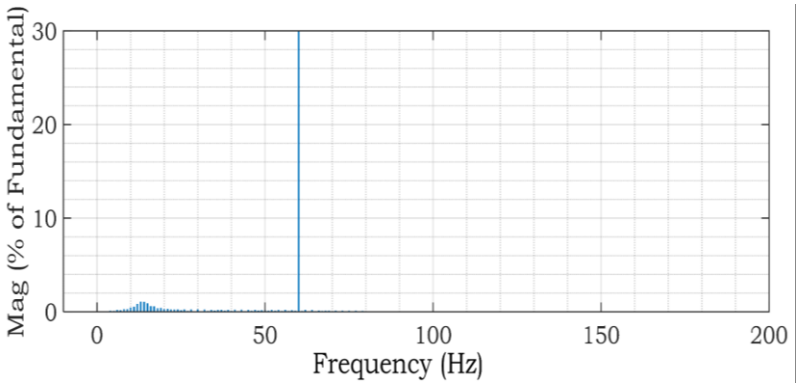

(b)

Fig.3-23. Time domain simulation results after using DSOGI-PLL,

(a) grid voltage waveform, (b) harmonics analysis result.

By comparing Fig. 3-11(a) with 3-23, we can find that by replacing the traditional SRF-PLL with SOGI-PLL block, a desirable SSR damping performance can be achieved. Therefore, SOGI-PLL could be an ideal alternative to conventional SRF-PLL when facing the SSR problem.

From the above analysis, we can find that the both MAF-PLL and DSOGI-PLL can be good alternatives to traditional SRF-PLL. These advanced PLL technologies based on harmonic filtering can phase out the sub-synchronous components before the LPF in the SRF-PLL, to protect the output of PLL from containing sub-synchronous components, hence the multiple SSR frequencies issue brought by traditional SRF-PLL block can be eliminated. Therefore, the advanced PLL technologies can also be adopted in reality to help solve the SSR problem.

The restriction when using advanced PLL technologies to mitigate SSR oscillations should also be pointed out. In the above simulations, only one WTG is involved in the system, when the number of WTGs increases, the SSR damping performance of both the above two strategies will deteriorate badly. Fig. 3.24 shows the simulation results of GSC with SOGI-PLL, when the number of type 4 WTGs increases to five. And these simulation results are almost same as simulation results when the GSC employing a MAF-PLL.

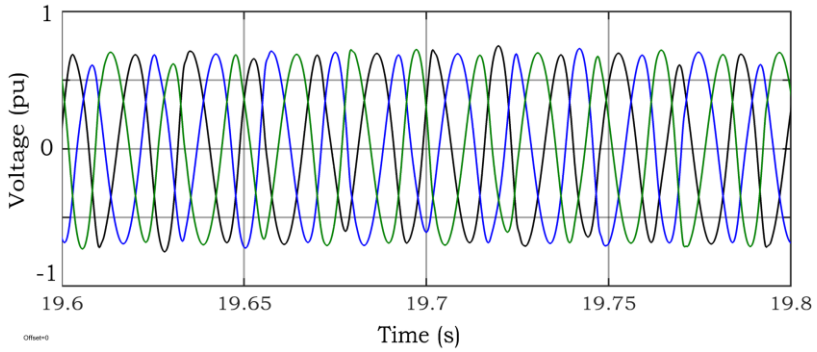

(a)

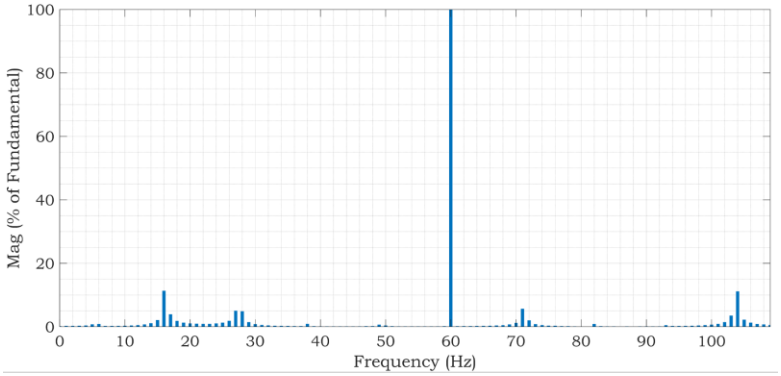

(b)

Fig.3-24. Time domain simulation results after using DSOGI-PLL with 5 WTGs in the system, (a) grid voltage waveform, (b) harmonics analysis result.

As can be seen from Figs. 3-24 (a) and (b), even with advanced PLL technology taking place of traditional SRF-PLL block, limited progress can be made in SSR damping. And the system still suffers from multiple SSR frequencies problem.

Although advanced PLL technologies are capable to help alleviate SSR oscillations and solve the multiple SSR frequency problem brought by traditional SRF-PLL. Its SSR damping capability

is still limited when facing large WFs based on type 4 WTGs in the real world. Hence, it is suggested to combine the advanced PLLs with the control strategy suggested in Section 3.2, i.e. *P* + *Q* control in GSC to achieve a better SSR damping performance in practical application scenarios.

3.4 Summary

In this chapter, the existing SSR damping schemes in WFs based on type 3 and type 4 WTGs are compared and improved SSR damping methods are proposed, which are supported by the simulations in both frequency- and time-domains.

First, for WFs based on type 3 WTGs, the virtual impedance method cannot achieve an admiring SSR mitigation performance. A better alternative could be utilizing STATCOM devices with SSRDC. However, the SSR damping capability of this method is still limited due to the incapability of active power control of STATCOM devices. Hence, the STATCOM with ESS would be better to be utilized in SSR damping.

Second, for WFs based on Type 4 WTGs, four types of existing VSC control strategies have been analyzed with special attention on their SSR oscillation mitigation potential and damping properties. As shown in this chapter the VSC with the direct active and reactive power control strategy has a much better damping performance compared to the scheme having voltage control in the outer loop.

Third, the impact of PLL block in SSR oscillations are discussed. And the SSR damping scheme by using advanced PLL technologies is proposed. By replacing the traditional SRF-PLL with advanced PLL technologies, i.e. MAF-PLL and SOGI-PLL, a desirable SSR damping performance can be achieved.

Chapter 4
Conclusions and Recommendation

4.1 Conclusions

As SSR oscillations have been observed in WFs based on VSWTGs and have caused series damage and tripping of WFs, therefore, SSR problems should be investigated. The mechanisms of SSR should be studied and clarified and consequently proper mitigation methods can be proposed to solve this problem.

In this dissertation, the SSR oscillations in WFs based on VSWTGs have been investigated in detail. First a comprehensive review of SSR has been done to identify the mechanisms, impact factors of SSR in WFs based on type 3 and type 4 WTGs. Then existing damping schemes are evaluated and compared. Based on existing methods, improved SSR damping methods have been proposed. The main topic covers the root cause identification, impedance model-based analysis, influence factors and existing and potential improved mitigation methods in WFs based on type 3, type 4 WTGs and in WFs with HVDC connection.

Based on the impedance model, we can conclude the essential cause of the SSR issue in WFs is the negative equivalent resistance. For a type 3 WTG-based WF, the negative equivalent resistance of the WF is due to the slip; for a type 4 WTG-based WF, the negative equivalent resistance is generated by the GSC; for an interconnected system with WFs and HVDC transmission systems, the SEC of the HVDC also has a negative equivalent resistance. The negative equivalent resistance will provide negative damping to SSR oscillations. Therefore, all these systems have a potential to suffer the SSR problem.

The different impedance properties of WFs, whether inductive (type 3 WTG-based WFs) or capacitive (type 4 WTG-based WFs), dominate the external triggers for SSR oscillations, i.e. whether series compensation networks (type 3 WTG-based WFs) or weak grids (type 4 WTG-based WFs). HVDC transmission system interacts with WFs based on both type 3 and 4 WTGs

since it has either inductive or capacitive impedance characteristics in the different frequency. Moreover, the PLL block in the GSC could potentially cause multiple SSR frequencies problem.

The existing SSR mitigation schemes have been investigated in detail and improved methods have been proposed. For WFs based on type 3 WTGs, the SSR damping performance of existing virtual impedance schemes are limited. The STATCOM with SSRDC could be an alternative for SSR mitigation. STATCOM devices provide more positive damping when adopting the reactive power control on the *q*-axis of the control loop rather than using PCC voltage control. Besides, an admiring SSR mitigation performance could achieve when STATCOM with SSRDC signals integrated in both *d*- and *q*-axes. In this way, traditional STATCOM devices which are not capable to control active power flow may show a limited SSR damping performance in large WFs systems. Therefore, STATCOM with ESS is viable option that can be considered to damp SSR oscillations.

For WFs based on Type 4 WTGs, the existing VSC control strategies have been analyzed with special attention on their SSR oscillation mitigation potential and damping properties. The study shows that the VSC with the direct active and reactive power control strategy has a much better damping performance compared to the scheme having voltage control in the outer loop.

The multiple SSR frequencies issue caused by traditional SRF-PLL on SSR oscillations are investigated. And advanced three-phase PLL technologies based on overall harmonic detection technology are studied and utilized to avoid the inferences brought by SRF-PLL block. Two representative PLL technologies based on overall harmonic detection technology, i.e. MAF-PLL and SOGI-PLL are studied in detail. These advanced PLL technologies are capable to solve the multiple SSR frequencies issue brought by conventional SRF-PLL.

4.2 Recommendations

The following work is suggested for future research.

1) Enhance the capability of STATCOM in SSR damping with ESS

As discussed in Section 3.1, the capability of STATCOM in SSR damping is limited since in STATCOM devices only the *q*-axis is utilized to inject SSR damping, which is not large enough

for large WFs. Therefore, STATCOM with ESS is viable options that can be considered to improve the capability of STATCOM to damp SSR oscillations.

2) Coordinated control of WFs and HVDC systems

As discussed in Section 2.4, it becomes complex when studying SSR oscillations between WFs and HVDC systems, as the VSCs on both sides should be concerned. That is the interaction between the GSC of type 4 WTGs and the SEC of HVDC systems should be considered. And the control strategies of VSC impact the SSR damping performance which has been discussed in Section 3.2. Therefore, the coordinated control of both WFs and HVDC systems should be considered to avoid SSR oscillations.

References

[1] K. Ohlenforst, S. Sawyer, A. Dutton, B. Backwell, and etc. (2016, Oct.). “Global Wind Report 2018”. Global Wind Energy Council, Brussels, BE. [Online]: Available: https://gwec.net/wp-content/uploads/2019/04/GWEC-Global-Wind-Report-2018.pdf.

[2] P. Pourbeik. “Proposed Changes to the WECC WT4 Generic Model for Type 4 Wind Turbine Generators”. EPRI, Palo Alto, CA: 2011, 1021763. (available for free download at www.epri.com)

[3] J. Adams, C. Carter and S. Huang, "ERCOT experience with Sub-synchronous Control Interaction and proposed remediation," *PES T&D* 2012, Orlando, FL, 2012, pp. 1-5.

[4] X. Xie, X. Zhang, H. Liu, H. Liu, Y. Li and C. Zhang, "Characteristic Analysis of Subsynchronous Resonance in Practical Wind Farms Connected to Series-Compensated Transmissions," in *IEEE Transactions on Energy Conversion*, vol. 32, no. 3, pp. 1117-1126, Sept. 2017.

[5] L. Wang, X. Xie, Q. Jiang, H. Liu, Y. Li and H. Liu, "Investigation of SSR in Practical DFIG-Based Wind Farms Connected to a Series-Compensated Power System," in *IEEE Transactions on Power Systems*, vol. 30, no. 5, pp. 2772-2779, Sept. 2015.

[6] G.P. Chen, M. J. Li, T. Xu, eta al. “Study on Technical Bottleneck of New Energy Development [J]”. *Proceedings of the CSEE*, 2017, 37(1): 20-26(in Chinese).

[7] X.R. Xie, H. K. Liu, J.B. He, eta al. “Mechanism and Characteristics of Subsynchronous Oscillation Caused by the Interaction Between Full-converter Wind Turbines and AC Systems [J]”. *Proceedings of the CSEE*, 2016, 36(0): 1-7(in Chinese).

[8] H. Liu *et al*., "Subsynchronous Interaction Between Direct-Drive PMSG Based Wind Farms and Weak AC Networks," in *IEEE Transactions on Power Systems*, vol. 32, no. 6, pp. 4708-4720, Nov. 2017.

[9] W. Liu, X. Xie, H. Liu and J. He, "Mechanism and characteristic analyses of subsynchronous oscillations caused by the interactions between direct-drive wind turbines and weak AC power systems," in *The Journal of Engineering*, vol. 2017, no. 13, pp. 1651-1656, 2017.

[10] T. Bi, J. Li, P. Zhang, E. Mitchell-Colgan and S. Xiao, "Study on response characteristics of grid-side converter controller of PMSG to sub-synchronous frequency component," in *IET Renewable Power Generation*, vol. 11, no. 7, pp. 966-972, 7 6 2017.

[11] J. Lyu, X. Cai, M. Amin and M. Molinas, "Sub-synchronous oscillation mechanism and its suppression in MMC-based HVDC connected wind farms," in *IET Generation, Transmission & Distribution*, vol. 12, no. 4, pp. 1021-1029, 27 2 2018.

[12] K.R.Padiyar, *Analysis of subsynchronous resonance in power systems*. India: Bangalore, 1999.

[13] A. Moharana, R. K. Varma and R. Seethapathy, "Modal analysis of Type-1 wind farm connected to series compensated transmission line and LCC HVDC transmission line," 2012 *IEEE Electrical Power and Energy Conference*, London, ON, 2012, pp. 202-209.

[14] A. Moharana and R. K. Varma, "Subsynchronous resonance in single-cage self-excited-induction-generator-based wind farm connected to series-compensated lines," in *IET Generation, Transmission & Distribution*, vol. 5, no. 12, pp. 1221-1232, December 2011.

[15] R. K. Varma and A. Moharana, "SSR in Double-Cage Induction Generator-Based Wind Farm Connected to Series-Compensated Transmission Line," in *IEEE Transactions on Power Systems*, vol. 28, no. 3, pp. 2573-2583, Aug. 2013.

[16] A. E. Leon and J. A. Solsona, "Sub-Synchronous Interaction Damping Control for DFIG Wind Turbines," in *IEEE Transactions on Power Systems*, vol. 30, no. 1, pp. 419-428, Jan. 2015.

[17] L. Fan, C. Zhu, Z. Miao and M. Hu, "Modal Analysis of a DFIG-Based Wind Farm Interfaced With a Series Compensated Network," in *IEEE Transactions on Energy Conversion*, vol. 26, no. 4, pp. 1010-1020, Dec. 2011.

[18] J. Sun, "Small-Signal Methods for AC Distributed Power Systems–A Review," in *IEEE Transactions on Power Electronics*, vol. 24, no. 11, pp. 2545-2554, Nov. 2009.

[19] Z. Miao, "Impedance-Model-Based SSR Analysis for Type 3 Wind Generator and Series-Compensated Network," in *IEEE Transactions on Energy Conversion*, vol. 27, no. 4, pp. 984-991, Dec. 2012.

[20] Y. Song, X. Wang and F. Blaabjerg, "Impedance-Based High-Frequency Resonance Analysis of DFIG System in Weak Grids," in *IEEE Transactions on Power Electronics*, vol. 32, no. 5, pp. 3536-3548, May 2017.

[21] I. Vieto and J. Sun, "Small-signal impedance modelling of type-III wind turbine," 2015 *IEEE Power & Energy Society General Meeting*, Denver, CO, 2015, pp. 1-5.

[22] J. Sun, "Impedance-Based Stability Criterion for Grid-Connected Inverters," in *IEEE Transactions on Power Electronics*, vol. 26, no. 11, pp. 3075-3078, Nov. 2011.

[23] Lingling Fan and Zhixin Miao, "Nyquist stability criterion based ssr explanation for type 3 wind generators," 2013 *IEEE Power & Energy Society General Meeting*, Vancouver, BC, 2013, pp. 1-1

[24] J. Sun, "Impedance-Based Stability Criterion for Grid-Connected Inverters," in *IEEE Transactions on Power Electronics*, vol. 26, no. 11, pp. 3075-3078, Nov. 2011.

[25] N. Johansson, L. Angquist and H. Nee, "A Comparison of Different Frequency Scanning Methods for Study of Subsynchronous Resonance," in *IEEE Transactions on Power Systems*, vol. 26, no. 1, pp. 356-363, Feb. 2011.

[26] D. H. Suriyaarachchi, U. Annakkage, C. Karawita and D. Jacobson, "A procedure to study sub-synchronous interactions in wind integrated power systems," 2013 IEEE Power & Energy Society General Meeting, Vancouver, BC, 2013, pp. 1-1.

[27] N. Cao, K. Chong, L. Qi, D. Jin and Z. Song, "Impedance-based analysis on subsynchronous oscillation mechanism caused of VSC-HVDC with double-fed induction generator," 2017 *Chinese Automation Congress (CAC)*, Jinan, 2017, pp. 3602-3608.

[28] J. Lyu, X. Cai and M. Molinas, "Optimal Design of Controller Parameters for Improving the Stability of MMC-HVDC for Wind Farm Integration," in *IEEE Journal of Emerging and Selected Topics in Power Electronics*, vol. 6, no. 1, pp. 40-53, March 2018.

[29] J. Lyu, X. Cai and M. Molinas, "Frequency Domain Stability Analysis of MMC-Based HVdc for Wind Farm Integration," in *IEEE Journal of Emerging and Selected Topics in Power Electronics*, vol. 4, no. 1, pp. 141-151, March 2016.

[30] M. Amin and M. Molinas, "Understanding the Origin of Oscillatory Phenomena Observed Between Wind Farms and HVdc Systems," in *IEEE Journal of Emerging and Selected Topics in Power Electronics*, vol. 5, no. 1, pp. 378-392, March 2017.

[31] C. Zhang, W. S. Wang, G. Q. He, eta al. “Analysis of Sub-synchronous oscillation of full-converter wind farm based on sequence impedance and an optimized design method for PLL parameters [J]”. *Proceedings of the CSEE*, 2017, 37(23): 6757-6767(in Chinese).

[32] Gao Feng, He Qifei, Hao Zhiguo and Zhang Baohui, "The research of sub synchronous oscillation in PMSG wind farm," 2016 *IEEE PES Asia-Pacific Power and Energy Engineering Conference (APPEEC)*, Xi'an, 2016, pp. 1883-1887.

[33] L. Fan and Z. Miao, "Mitsigating SSR Using DFIG-Based Wind Generation," in *IEEE Transactions on Sustainable Energy*, vol. 3, no. 3, pp. 349-358, July 2012.

[34] S. O. Faried, I. Unal, D. Rai and J. Mahseredjian, "Utilizing DFIG-Based Wind Farms for Damping Subsynchronous Resonance in Nearby Turbine-Generators," in *IEEE Transactions on Power System*s, vol. 28, no. 1, pp. 452-459, Feb. 2013.

[35] X. Gao, U. Karaagac, S. O. Faried and J. Mahseredjian, "On the use of wind energy conversion systems for mitigating subsynchronous resonance and subsynchronous interaction," *IEEE PES Innovative Smart Grid Technologies*, Europe, Istanbul, 2014, pp. 1-6.

[36] H. A. Mohammadpour and E. Santi, "SSR Damping Controller Design and Optimal Placement in Rotor-Side and Grid-Side Converters of Series-Compensated DFIG-Based Wind Farm," in *IEEE Transactions on Sustainable Energy*, vol. 6, no. 2, pp. 388-399, April 2015.

[37] I. Vieto and J. Sun, "Damping of subsynchronous resonance involving Type-III wind turbines," 2015 *IEEE 16th Workshop on Control and Modeling for Power Electronics (COMPEL)*, Vancouver, BC, 2015, pp. 1-8.

[38] J. Lyu, M. Molinas and X. Cai, "Stabilization control methods for enhancing the stability of wind farm integration via an MMC-based HVDC system," 2017 *11th IEEE International Conference on Compatibility, Power Electronics and Power Engineering (CPE-POWERENG)*, Cadiz, 2017, pp. 324-329.

[39] L. Piyasinghe, Zhixin Miao, J. Khazaei and Lingling Fan, "Impedance model-based SSR analysis for TCSC compensated type-3 wind energy delivery systems," 2015 *IEEE Power & Energy Society General Meeting*, Denver, CO, 2015, pp. 1-1.

[40] H. A. Mohammadpour, J. Siegers and E. Santi, "Controller design for TCSC using observed-state feedback method to damp SSR in DFIG-based wind farms," 2015 *IEEE Applied Power Electronics Conference and Exposition (APEC)*, Charlotte, NC, 2015, pp. 2993-2998.

[41] H. A. Mohammadpour, M. M. Islam, D. Coats, E. Santi and Y. J. Shin, "Sub-synchronous resonance mitigation in wind farms using gate-controlled series capacitor," 2013 *4th IEEE International Symposium on Power Electronics for Distributed Generation Systems (PEDG)*, Rogers, AR, 2013, pp. 1-6.

[42] H. A. Mohammadpour, Y. J. Shin and E. Santi, "SSR analysis of a DFIG-based wind farm interfaced with a gate-controlled series capacitor," 2014 *IEEE Applied Power Electronics Conference and Exposition - APEC* 2014, Fort Worth, TX, 2014, pp. 3110-3117.

[43] A. Moharana, R. Varma and R. Seethapathy, "SSR alleviation by STATCOM in induction generator based wind farm connected to series compensated line," 2014 *IEEE PES T&D Conference and Exposition*, Chicago, IL, USA, 2014, pp. 1-1.

[44] S. Golshannavaz, M. Mokhtari and D. Nazarpour, "SSR suppression via STATCOM in series compensated wind farm integrations," 2011 *19th Iranian Conference on Electrical Engineering*, Tehran, 2011, pp. 1-1.

[45] M. S. El Moursi and V. Khadkikar, "Novel control strategies for SSR mitigation and damping power system oscillations in a series compensated wind park," IECON 2012 - *38th Annual Conference on IEEE Industrial Electronics Society*, Montreal, QC, 2012, pp. 5335-5342.

[46] Y. Zhang, X. Chen and J. Sun, "Impedance modeling and control of STATCOM for damping renewable energy system resonance," 2017 *IEEE Energy Conversion Congress and Exposition (ECCE)*, Cincinnati, OH, 2017, pp. 3295-3302.

[47] S. F. Torabi, D. Nazarpour and Y. Shayestehfard, "Mitigation of subsynchronous resonance by static compensator with the aid of fuzzy logic controller and adaptive neuro fuzzy

inference system controller," 2012 Proceedings of *17th Conference on Electrical Power Distribution*, Tehran, 2012, pp. 1-5.

[48] H. A. Mohammadpour and E. Santi, "Sub-synchronous resonance analysis in DFIG-based wind farms: Definitions and problem identification — Part I," 2014 *IEEE Energy Conversion Congress and Exposition (ECCE)*, Pittsburgh, PA, 2014, pp. 812-819.

[49] H. A. Mohammadpour and E. Santi, "Sub-synchronous resonance analysis in DFIG-based wind farms: Mitigation methods — TCSC, GCSC, and DFIG controllers — Part II," 2014 *IEEE Energy Conversion Congress and Exposition (ECCE)*, Pittsburgh, PA, 2014, pp. 1550-1557.

[50] Graham Rogers, *Power system oscillations*. USA: New York, 2000.

[51] H. A. Mohammadpour and E. Santi, "SSR Damping Controller Design and Optimal Placement in Rotor-Side and Grid-Side Converters of Series-Compensated DFIG-Based Wind Farm," in *IEEE Transactions on Sustainable Energy*, vol. 6, no. 2, pp. 388-399, April 2015.

[52] Xiaogang Feng, Jinjun Liu and F. C. Lee, "Impedance specifications for stable DC distributed power systems," in *IEEE Transactions on Power Electronics*, vol. 17, no. 2, pp. 157-162, March 2002.

[53] K. M. Alawasa, Y. A. I. Mohamed and W. Xu, "Modeling, Analysis, and Suppression of the Impact of Full-Scale Wind-Power Converters on Subsynchronous Damping," in *IEEE Systems Journal*, vol. 7, no. 4, pp. 700-712, Dec. 2013.

[54] L. Harnefors, M. Bongiorno and S. Lundberg, "Input-Admittance Calculation and Shaping for Controlled Voltage-Source Converters," in *IEEE Transactions on Industrial Electronics*, vol. 54, no. 6, pp. 3323-3334, Dec. 2007.

[55] R. D. Middlebrook, "Small-signal modeling of pulse-width modulated switched-mode power converters," in *Proceedings of the IEEE*, vol. 76, no. 4, pp. 343-354, April 1988.

[56] H. Liu and J. Sun, "Voltage Stability and Control of Offshore Wind Farms With AC Collection and HVDC Transmission," in *IEEE Journal of Emerging and Selected Topics in Power Electronics*, vol. 2, no. 4, pp. 1181-1189, Dec. 2014.

[57] "First benchmark model for computer simulation of subsynchronous resonance," in *IEEE Transactions on Power Apparatus and Systems*, vol. 96, no. 5, pp. 1565-1572, Sept. 1977.

[58] Y. W. Li and C. Kao, "An Accurate Power Control Strategy for Power-Electronics-Interfaced Distributed Generation Units Operating in a Low-Voltage Multibus Microgrid," in *IEEE Transactions on Power Electronics*, vol. 24, no. 12, pp. 2977-2988, Dec. 2009.

[59] H. A. Mohammadpour and E. Santi, "Optimal adaptive sub-synchronous resonance damping controller for a series-compensated doubly-fed induction generator-based wind farm," in *IET Renewable Power Generation*, vol. 9, no. 6, pp. 669-681, 8 2015.

[60] Gao Feng, He Qifei, Hao Zhiguo and Zhang Baohui, "The research of sub synchronous oscillation in PMSG wind farm," 2016 *IEEE PES Asia-Pacific Power and Energy Engineering Conference (APPEEC)*, Xi'an, 2016, pp. 1883-1887.

[61] L. Fan and Z. Miao, "Wind in Weak Grids: 4 Hz or 30 Hz Oscillations?" in *IEEE Transactions on Power Systems*, vol. 33, no. 5, pp. 5803-5804, Sept. 2018.

[62] K. M. Alawasa, Y. A. I. Mohamed and W. Xu, "Active Mitigation of Subsynchronous Interactions Between PWM Voltage-Source Converters and Power Networks," in *IEEE Transactions on Power Electronics*, vol. 29, no. 1, pp. 121-134, Jan. 2014.

[63] L. Xu and L. Fan, "Impedance-Based Resonance Analysis in a VSC-HVDC System," in *IEEE Transactions on Power Delivery*, vol. 28, no. 4, pp. 2209-2216, Oct. 2013.

[64] M. Amin, M. Molinas and J. Lyu, "Oscillatory phenomena between wind farms and HVDC systems: The impact of control," *2015 IEEE 16th Workshop on Control and Modeling for Power Electronics (COMPEL)*, Vancouver, BC, 2015, pp. 1-8.

[65] J. Lyu and X. Cai, "Impact of controller parameters on stability of MMC-based HVDC systems for offshore wind farms," *International Conference on Renewable Power Generation (RPG 2015)*, Beijing, 2015, pp. 1-6.

[66] M. P. Bahrman and B. K. Johnson, "The ABCs of HVDC transmission technologies," in *IEEE Power and Energy Magazine*, vol. 5, no. 2, pp. 32-44, March-April 2007.

[67] Y. Cheng, C. Qian, M. L. Crow, S. Pekarek and S. Atcitty, "A Comparison of Diode-Clamped and Cascaded Multilevel Converters for a STATCOM With Energy Storage," in *IEEE Transactions on Industrial Electronics*, vol. 53, no. 5, pp. 1512-1521, Oct. 2006.

[68] B. Wen, D. Dong, D. Boroyevich, R. Burgos, P. Mattavelli and Z. Shen, "Impedance-Based Analysis of Grid-Synchronization Stability for Three-Phase Paralleled Converters," in *IEEE Transactions on Power Electronics*, vol. 31, no. 1, pp. 26-38, Jan. 2016.

[69] X. Yuan, F. Wang, D. Boroyevich, Y. Li and R. Burgos, "DC-link Voltage Control of a Full Power Converter for Wind Generator Operating in Weak-Grid Systems," in *IEEE Transactions on Power Electronics*, vol. 24, no. 9, pp. 2178-2192, Sept. 2009.

[70] H. Liu, X. Xie and W. Liu, "An Oscillatory Stability Criterion Based on the Unified dq -Frame Impedance Network Model for Power Systems With High-Penetration Renewables," in *IEEE Transactions on Power Systems*, vol. 33, no. 3, pp. 3472-3485, May 2018.

[71] V. Kaura and V. Blasko, "Operation of a phase locked loop system under distorted utility conditions," in *IEEE Transactions on Industry Applications*, vol. 33, no. 1, pp. 58-63, Jan.-Feb. 1997.

[72] L. Asiminoaei, S. Kalaschnikow and S. Hansen, "Overall and selective compensation of harmonic currents in Active Filter applications," 2009 *Compatibility and Power Electronics*, Badajoz, 2009, pp. 153-160.

[73] K. Sergej, L. Asiminoaei and S. Hansen, "Harmonic detection methods of active filters for adjustable speed drive applications," 2009 *13th European Conference on Power Electronics and Applications*, Barcelona, 2009, pp. 1-10.

[74] H. Akagi, S. Ogasawara and Hyosung Kim, "The theory of instantaneous power in three-phase four-wire systems: a comprehensive approach," Conference Record of the 1999 *IEEE Industry Applications Conference.* Thirty-Forth IAS Annual Meeting (Cat. No.99CH36370), Phoenix, AZ, USA, 1999, pp. 431-439 vol.1.

[75] S. Golestan, M. Ramezani, J. M. Guerrero, F. D. Freijedo and M. Monfared, "Moving Average Filter Based Phase-Locked Loops: Performance Analysis and Design Guidelines," in *IEEE Transactions on Power Electronics*, vol. 29, no. 6, pp. 2750-2763, June 2014.

[76] S. Golestan, J. M. Guerrero and A. M. Abusorrah, "MAF-PLL With Phase-Lead Compensator," in *IEEE Transactions on Industrial Electronics*, vol. 62, no. 6, pp. 3691-3695, June 2015.

[77] J. Wang, J. Liang, F. Gao, L. Zhang and Z. Wang, "A Method to Improve the Dynamic Performance of Moving Average Filter-Based PLL," in *IEEE Transactions on Power Electronics*, vol. 30, no. 10, pp. 5978-5990, Oct. 2015.

[78] F. D. Freijedo, J. Doval-Gandoy, O. Lopez and E. Acha, "Tuning of Phase-Locked Loops for Power Converters Under Distorted Utility Conditions," in *IEEE Transactions on Industry Applications*, vol. 45, no. 6, pp. 2039-2047, Nov.-dec. 2009.

[79] P. Xiao, K. A. Corzine and G. K. Venayagamoorthy, "Multiple Reference Frame-Based Control of Three-Phase PWM Boost Rectifiers under Unbalanced and Distorted Input Conditions," in *IEEE Transactions on Power Electronics*, vol. 23, no. 4, pp. 2006-2017, July 2008.

[80] K. Martin, “Complex signal processing is not complex,” *IEEE Trans. Circuits Syst. I, Reg. Papers*, vol. 51, no. 9, pp. 1823–1836, Sep. 2004.

[81] Y. F. Wang and Y. Wei Li, "Analysis and Digital Implementation of Cascaded Delayed-Signal-Cancellation PLL," in *IEEE Transactions on Power Electronics*, vol. 26, no. 4, pp. 1067-1080, April 2011.

[82] Y. F. Wang and Y. W. Li, "Three-Phase Cascaded Delayed Signal Cancellation PLL for Fast Selective Harmonic Detection," *in IEEE Transactions on Industrial Electronics*, vol. 60, no. 4, pp. 1452-1463, April 2013.

[83] Y. F. Wang and Y. W. Li, "Grid Synchronization PLL Based on Cascaded Delayed Signal Cancellation," in *IEEE Transactions on Power Electronics*, vol. 26, no. 7, pp. 1987-1997, July 2011.

[84] M. Ciobotaru, R. Teodorescu and F. Blaabjerg, "A new single-phase PLL structure based on second order generalized integrator," 2006 37*th IEEE Power Electronics Specialists Conference*, Jeju, 2006, pp. 1-6.

[85] P. Rodríguez, A. Luna, R. S. Muñoz-Aguilar, I. Etxeberria-Otadui, R. Teodorescu and F. Blaabjerg, "A Stationary Reference Frame Grid Synchronization System for Three-Phase

Grid-Connected Power Converters Under Adverse Grid Conditions," in *IEEE Transactions on Power Electronics*, vol. 27, no. 1, pp. 99-112, Jan. 2012.

[86] P. Rodríguez, R. Teodorescu, I. Candela, A. V. Timbus, M. Liserre and F. Blaabjerg, "New positive-sequence voltage detector for grid synchronization of power converters under faulty grid conditions," 2006 *37th IEEE Power Electronics Specialists Conference*, Jeju, 2006, pp. 1-7.